UNIVERSITY of OULU
OULUN YLIOPISTO

DEGREE PROGRAM IN WIRELESS COMMUNICATION ENGINEERING

MASTER'S THESIS

CHARACTERIZING NONLINEARITY IN MULTIANTENNA MULTIBEAM TRANSMITTERS

Author	Muhammad Yasir Javed
Supervisor	Aarno Parssinen
Second Examiner	Timo Rahkonen
Tecnical Advisor	Nuutti Tervo

November 2017

M. Javed (2017) Characterizing nonlinearity in multiantenna multibeam transmitters. University of Oulu, Department of Information Technology and Electrical Engineering, Degree Program in Wireless Communications Engineering. Master's thesis, 53 p.

ABSTRACT

In this thesis, effects of power amplifier (PA) distortion in multiantenna transmitter is studied. Input signal of each PA in the array is modelled by two or multiple tones to characterize the nonlinearity in terms of intermodulation distortion (IMD). In intermodulation, the phase of the nonlinearity depends on the phases of the corresponding input tones. Hence, in beamforming, progressive phase of the nonlinear components over the antenna elements creates a steered beam for the nonlinearity. Measurement setup is created to measure the phase and amplitude of the IMD components in the PA output. The theoretical polynomial relation of the IMD phase dependency on the input tones is validated by measurements. For flexible measurements, the setup is automatized by standard commands for programmable instruments.

Second part of the thesis studies the array IMD by simulations in MATLAB. The used PA model is a memoryless polynomial fitted against the measured amplitude-to-amplitude modulation and amplitude-to-phase modulation responses of a real amplifier. The effects of nonlinearity are studied by using two tones to present each independent data stream in the PA inputs. Hence, in multibeam scenario, each data stream is modelled by two tones having individual phase and amplitude depending on the beamforming coefficients of given stream. The simulations are performed in frequency domain by utilizing the concept of spectral convolution to model the intermodulation distortion, and array factor to model the far-field radiation of the linear and nonlinear PA output components. By utilizing the simulator, PA nonlinearity is analyzed in single-beam and multi-beam scenarios by varying the steering angles, allocated stream powers and amplitude distribution over the PAs. It is observed that IMD terms which depend on only one stream are steered to same direction as the linear terms whereas the IMD terms depending on both streams spreads more in space. This has potentially positive impacts on the signal-to-distortion ratio of the streams observed in beamforming directions.

Keywords: power amplifier, multiantenna, beamforming, multibeam, intermodulation

TABLE OF CONTENTS

FOREWORD

First of all, thanks to Allah, the almighty, for giving me strength to complete this thesis and for blessing me with many great people who have been greatest support in both my personal and professional life. I would like to seize this opportunity to express my deepest regards and gratitude to my technical advisor Ms. Sc. (Tech) Nuutti Tervo for his dedication and sincere efforts throughout the whole time. He has been my role model who I have always admired. I was really lucky and blessed to be taught by such a passionate and dedicated person to science.

I would also like to thank Professor Aarno Parssinen for the opportunity, trust and guidance. I would also like to extend my sincere appreciation to Professor Timo Rahkonen for being the second examiner of the thesis. Furthermore, I would like to thank all the Centre for Wireless Communications staff, my parents, family and friends for their support and love.

Oulu, Finland November 24, 2017

Muhammad Yasir Javed

LIST OF ABBREVIATIONS AND SYMBOLS

3G	third generation
4G	fourth generation
5G	fifth generation
ACPR	adjacent-channel-power-ratio
ADC	analog-to-digital converter
AF	array factor
AM-AM	amplitude-to-amplitude modulation
AM-PM	amplitude-to-phase modulation
cm	centimeter
CW	continuous wave
DAC	digital-to-analog converter
dB	decibel
dBm	decibels relative to milliwatt
DC	direct current
DUT	device under test
EIRP	effective isotropic radiated power
EM	electromagnetic
EVM	error vector magnitude
FE	front end
FOM	figure of merit
FSPL	free space path loss
FNBW	first null beamwidth
GHz	gigahertz
HPBW	half power beamwidth
IBI	inter-beam-interference
IF	intermediate frequency
IMD	intermodulation distortion
IM3H	third-order higher intermodulation term
IM3L	third-order lower intermodulation term
IP3	third-order intercept point
IQ	in-phase and quadrature
LO	local oscillator
LNA	low noise amplifier
MIMO	multiple-input-multiple-output
MIMR	multitone-intermodulation-ratio
mmWave	millimeter wave
MU-MIMO	multi-user multiple-input-multiple-output
NPR	noise power ratio
P1dB	1 dB compression point
PA	power amplifier
PAE	power added efficiency
PAPR	peak-to-average power ratio
Q-point	quiescent point
QAM	quadrature amplitude modulation
QPSK	quadrature phase shift keying

RF	radio frequency
RMS	root mean square
SCPI	standard commands for programmable instruments
SINR	signal-to-interference-plus-noise-ratio
SLL	sidelobe level
T/R	transmit / receive
TX	transmitter
VCO	voltage control oscillator
VGA	variable gain amplifier

$ACPR_l$	lower adjacent-channel-power-ratio
$ACPR_u$	upper adjacent-channel-power-ratio
A_{tone}	tone amplitude
$A_{tone-amp}$	amplified tone amplitude
b_1	first-order nonlinear coefficient
b_3	third-order nonlinear coefficient
b_5	fifth order nonlinear coefficient
b_n	n^{th} order power amplifier nonlinear term
b_{n1}	n^{th} antenna first-order nonlinear coefficient
b_{n3}	n^{th} antenna third-order nonlinear coefficient
b_{n5}	n^{th} antenna fifth order nonlinear coefficient
b_{nn}	n^{th} antenna n^{th} order nonlinear coefficient
d	antenna diameter
f_c	center frequency
f_{PAn}	nonlinear function of nth power amplifier
g_n	gain of n^{th} amplifier
IMD_L	lower intermodulation term
IMD_H	higher intermodulation term
k_x	x-component of wavevector
k_y	y-component of wavevector
k_z	z-component of wavevector
N_p	order of polynomial
P_{AVG}	average power
P_{DC}	direct current power
P_{error}	power value of error
P_{IN}	radio frequency input power
P_{IIP3}	power of input third-order intercept point
P_{OUT}	radio frequency output power
P_{PEAK}	peak power
$P_{reference}$	reference power
$\vec{r}$	position vector
R_1	radius of reactive near field region
R_2	radius of radiation near field region
V_{IN}	input voltage
V_{OUT}	output voltage
ω_n	n^{th} beamforming coefficient
X_{array}	array input

X_{array1}	array 1 input
X_{array2}	array 2 input
$X(f)$	input signal in frequency domain
X_n	n^{th} power amplfier input
y_n	n^{th} antenna coefficient

$\triangle f$	frequency offset
λ	wavelength
π	ratio of a circle's circumference to its diameter
θ	elevation angle in spherical coordinate system
θ_1	tone 1 phase
θ_2	tone 2 phase
θ_3	tone 3 phase
θ_4	tone 4 phase
ψ_n	phase progression of n^{th} antenna
ϕ_s	steering angle

1. INTRODUCTION

Key requirements for 5th generation (5G) mobile communication system are expected to have 10,000 times more traffic with 10-100 times more devices and latency of 1 millisecond (1 ms) or less compared to the present technologies. Present mobile technologies are not enough to meet the future mobile broadband demand of huge traffic and data rate. The present systems cannot be scaled to fulfill the needs for expected demands beyond 2020. To overcome the limitations, 5G mobile communication will be a combination of new technologies, new systems and new technical components [1]. Higher demand for traffic capacity and to support higher data rate, larger spectrum in sub-mmWave and mmWave regions must be utilized [2–5].

Radio wave propagation in sub-millimeter-wave (mmWave) and mmWave frequencies has new challenges for broadband communications. In general, path loss depends on frequency and distance. Furthermore, atmospheric loss, high penetration loss and frequency selective fading limit the communication in many scenarios [6, 7]. Larger path loss can be compensated either by increasing the transmit power or increasing the aperture size of the antenna [8–10]. Increasing transmit power is challenging in solid-state circuits because of the cost of gain and frequency dependent losses [11]. Also, power combining losses at mmWave frequencies are higher when multiple power producing devices are combined on chip or on printed circuit board (PCB); only limited number of power producing devices can be combined efficiently [12]. Another option to compensate larger path loss is to increase aperture size of the antenna (multiantenna systems).

Multiantenna systems use beamforming technique in which signals from multiple elements are combined over-the-air in certain direction [13, 14]. Improved signal-to-noise-ratio (SNR), higher capacity, low-loss power combining and spatial filtering are some of the benefits of beamforming. Beamforming is possible in fully analogue, fully digital or hybrid domain. Single-stream transmission in fully analogue and multi-stream transmission in fully digital system are possible but due to hardware complexity and power consumption at higher frequencies neither is very practical. Hybrid beamforming combines the advantages from both analogue and digital beamforming and provides higher system efficiency using normal hardware complexity and lower power consumption. In wideband mmWave systems, power-amplifiers (PAs) may not be the most power hungry devices anymore, but also analogue-to-digital converters (ADCs) / digital-to-analogue converters (DACs) are taking more power due to high sampling rates. Hence, hybrid/radio frequency (RF) beamforming is more attractive for implementation because of the lesser number of ADC/DAC [15].

In multiantenna systems, a power amplifier is needed separately for each antenna element. For amplifying the signals with high efficiency, power amplifiers are often working close to their nonlinear region, causing nonlinear distortion to the modulated waveform. Nonlinear behaviour of amplifier spreads some power into adjacent channel mainly due to intermodulation distortion. Most of the power in RF chain is consumed by the power amplifier. PA induced nonlinear distortions have substantial impact on the effective signal-to-interference-plus-noise-ratio (SINR) [12, 16]. Some portion of out-of-band distortion can be filtered out but in-band nonlinear distortion cannot because it lies in the same band as the useful signal, which decreases the SNR. In multiantenna

transmitters, in-band distortion from each antenna is radiated to the antenna far-field, which distorts the useful signal in same direction over-the-air.
In intermodulation, the phase of the nonlinearity depends on the phases of the corresponding input tones. In this thesis, relation is validated by measurements and the extracted AMAM and AMPM models are used to fit the nonlinear model. Measurement setup is created to measure the IMD phase and amplitude and the setup is automatized by SCPI commands. Simulation models in matlab are created to model the amplifiers and the antenna array. The nonlinearity of the PA is then analyzed in the array far-field in single-beam and multibeam scenarios. Scope of the thesis is shown in Figure 1

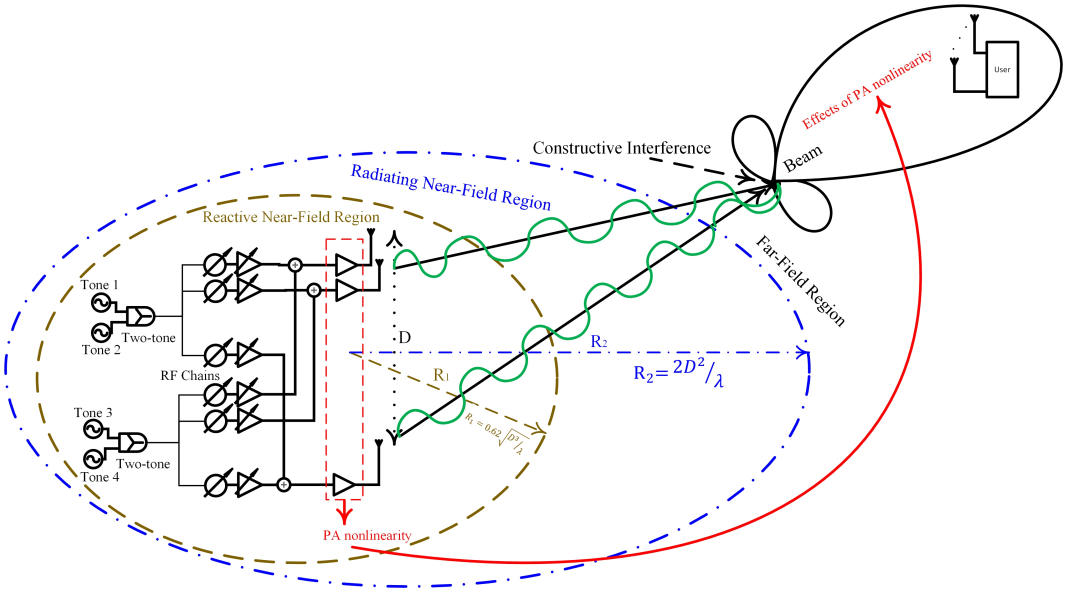

Figure 1. Scope of thesis.

This thesis is organized as follows. Chapter 2 studies sub-mmWave/mmWave propagation and antenna array modelling. Beamforming techniques, architectures, limitations and implementation challenges are also discussed in Chapter 2. Chapter 3 presents the nonlinear modelling of RF amplifier, intermodulation and harmonic distortion. Chapter 4 includes measurement techniques for characterizing PA nonlinearity. Finally, effects of PA array nonlinearity in single-beam and multibeam scenarios are discussed in Chapter 5.

2. BEAMFORMING ARCHITECTURES AND MODELLING

mmWave and sub-mmWave frequencies are highly interesting because of the wide available bandwidth enabling high data rate. Lower end of the millimeter-wave spectrum, just below 30 GHz is also chosen as one of the potential candidates for 5G mmWave systems. Multiantenna systems at mmWave band offer improved spectral efficiency, energy efficiency, higher array gain and higher capacity compared to the present systems. This chapter studies antenna array systems and beamforming architectures, and explains the array models which are utilized later on in this thesis. Furthermore, limitation and implementation challenges of beamforming architectures at mmWave frequencies are also briefly discussed.

2.1. Sub-millimeter and millimeter-wave frequencies

The sub-mmWave region of the electromagnetic spectrum is considered from 3 GHz to 30 GHz as shown in Figure 2. This band of frequencies is also known as the centimetre-wave band ranging wavelength from one to ten centimetres. Above the sub-mmWave band is the mmWave band, starting from 30 GHz and continuing up to 300 GHz.

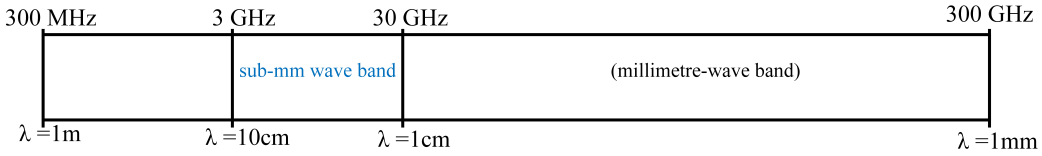

Figure 2. Sub-mmWave and mmWave spectrums.

These bands offer relatively wide available spectrum. Number of antennas can be increased significantly compared to third generation (3G) and fourth generation (4G) systems. Higher frequencies have bigger challenges for atmospheric attenuation at sub-mmWave and mmWave due to water vapour and gases in the air given in [17].

2.2. Antenna arrays and beamforming

Free space path loss (FSPL) is the loss in the signal strength which occurs when electromagnetic (EM) waves travel over the distance in free space without any obstacles in the path. Reason for FSPL is the spreading of the signal as it moves away from the source in the form of a sphere. Surface area of sphere increases and intensity of the signal decreases because it follows the law of conservation of energy. FSPL can be calculated as

$$FSPL = (4\pi d^2)(\frac{4\pi}{\lambda^2}), \tag{1}$$

where $4\pi d^2$ is spreading factor and $\frac{\lambda^2}{4\pi}$ is antenna effective area, d is distance of the receiver (Rx) from the transmitter (Tx) [m] and λ is the signal wavelength [m]. Wavelength at mmWave band is very small and hence mmWave signal has higher FSPL

compared to lower frequencies. Size of a radiator is proportional to wavelength. Also mmWave frequencies have bigger challenges for atmospheric attenuation due to water vapour and gases in the air given in [17]. To achieve high gain from the antenna, aperture size of the antenna should be very large. High gain antennas have narrow and fixed beams. Higher antenna gain can be achieved by increasing the number of elements to form an antenna array. Antenna array has radiating elements in a proper electrical and geometrical configuration, i.e. by increasing the antenna aperture shown in Figure 3.

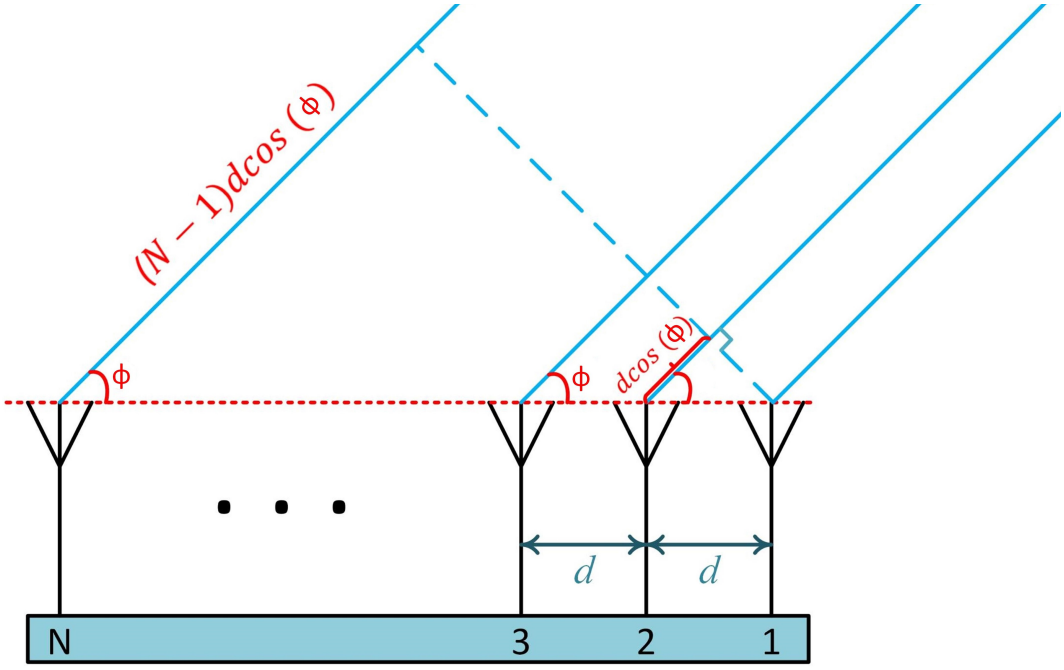

Figure 3. Uniform linear array (ULA) with N antenna elements, spaced uniformly with antenna spacing of d.

Usually, antenna elements considered to be identical because of the simplification of design and fabrication. The total radiated field of an array is a vector superposition of the fields radiated by the individual elements. To gain a very directive pattern from the antenna array, it is necessary that the fields generated by individual antenna elements should interfere constructively in the desired direction and interfere destructively in other directions. Overall, antenna pattern can be controlled by geometrical configuration of array, relative placement of antenna elements, excitation pattern of the individual elements and the individual pattern of each antenna [18].

2.2.1. Array factor

Array factor (AF) is a set of N identical omnidirectional antennas which face the same direction and follow an identical pattern. In general, AF depends on the number of elements, mutual placement, as well as the relative excitation of magnitudes and phases of individual elements. Array factor for N-element array can be calculated mathematically as

$$AF = \sum_{n=1}^{N} e^{-j\mathbf{k}\cdot\mathbf{r}_n}, \tag{2}$$

where N is the total number of antenna elements in the array, $\mathbf{r}_n$ is the relative placement of nth antenna in $[x, y, z]$ from the origin. $\mathbf{k}$ is the wave vector which describes the phase variation of a plane wave, in three orthogonal directions (x, y, and z-axes typically) and mathematically defined as

$$\mathbf{k} = (k_x, k_y, k_z) = \frac{2\pi}{\lambda}(sin\theta cos\phi, sin\theta sin\phi, cos\theta)\cdot \tag{3}$$

where θ is elevation angle and ϕ is azimuth angle. Magnitude of the wave vector will be equal to the wave-number as $k_x^2 + k_y^2 + k_z^2 = |\mathbf{k}|^2 = (\frac{2\pi}{\lambda})^2$. Polar plot of 8-element, $\lambda/2$-spaced horizontally aligned uniform linear array (ULA) at 30 GHz is shown in Figure 4.

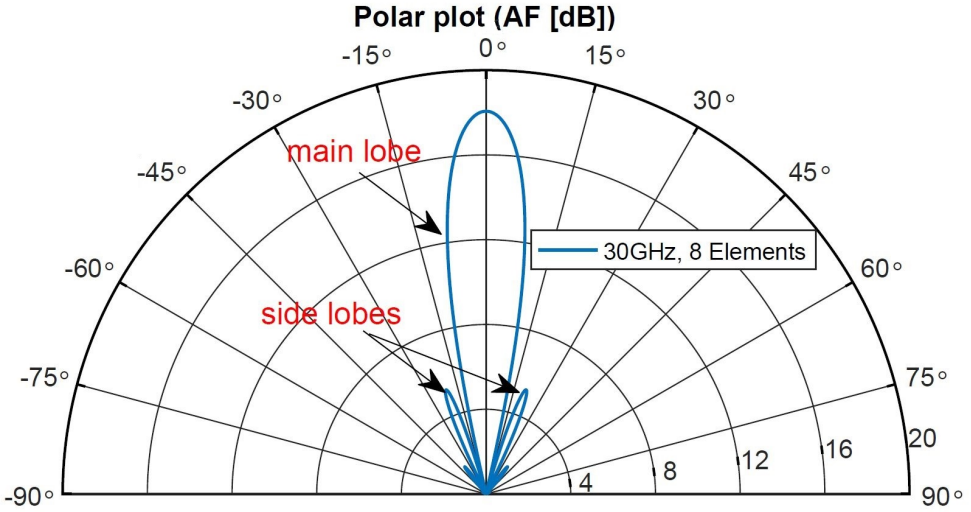

Figure 4. Polar plot of antenna array main lobe and sidelobes.

2.2.2. Sidelobe reduction

Array sidelobes can be reduced by amplitude distribution over the elements. In uniform amplitude distribution, amplitude coefficients are same for all elements of the array. Taylor coefficients allow to make trade-off between the main lobe width and the sidelobe level (SLL). The Taylor distribution avoids edge discontinuities, therefore Taylor window sidelobes decrease monotonically. Taylor amplitude distributions against antenna elements in array are shown in Figure 5, and Figure 6 shows the original sidelobe level and the sidelobe level with Taylor distribution.

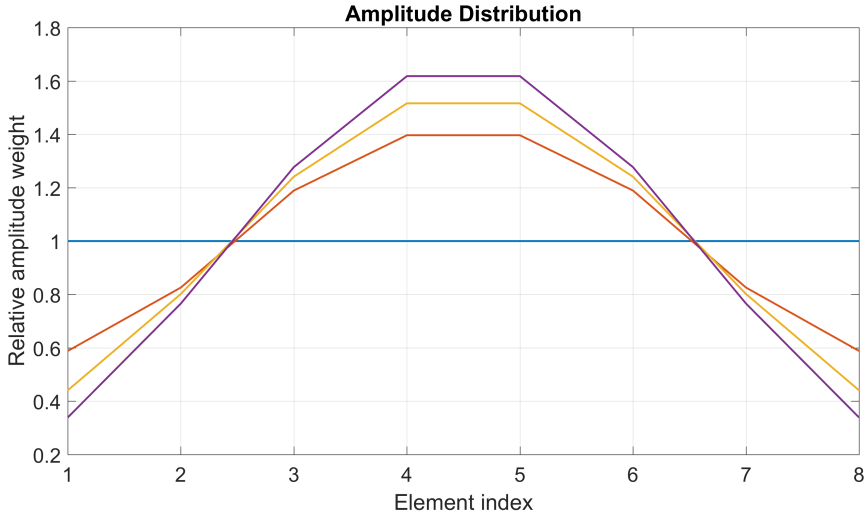

Figure 5. Taylor windows over the antenna elements for sidelobe reduction.

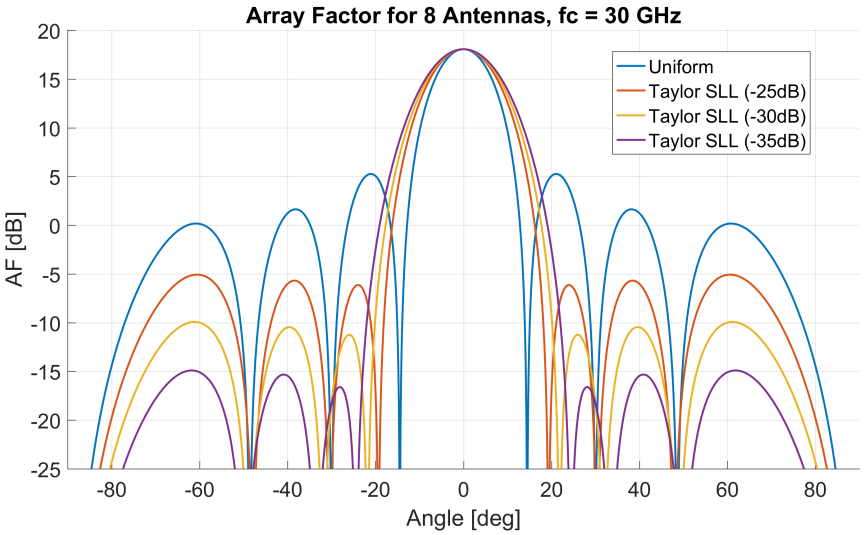

Figure 6. Sidelobe reduction with Taylor amplitude distribution.

2.2.3. Inter-element spacing

Array factor can get unwanted strong radiations as strong as array main beam in other directions, known as grating lobes. Usually, this occurs in uniformly spaced array elements, when inter-element spacing is too large. Spacing between adjacent elements should be less than or equal to half of the wavelength to avoid grating lobes. Array factor with different inter-element spacing and generation of grating lobes are demonstrated in Figure 7.

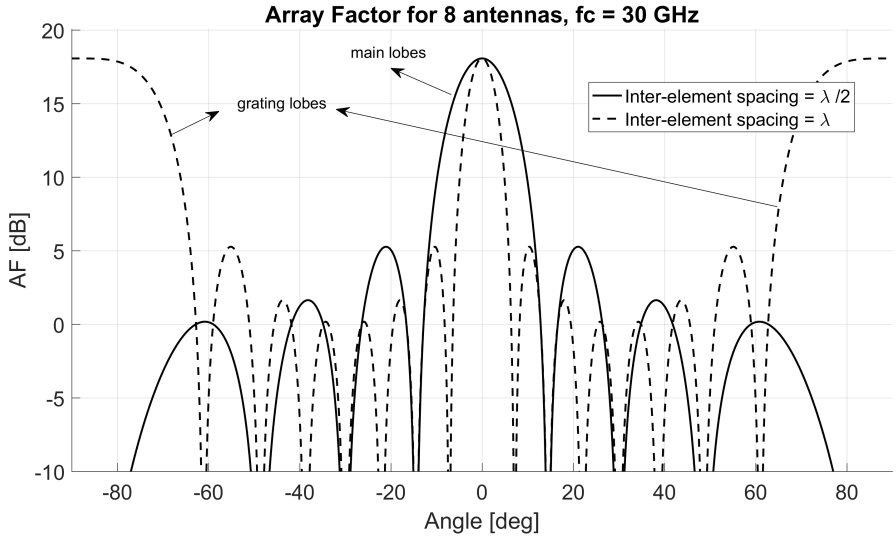

Figure 7. Array factor with different inter-element spacing.

2.2.4. Beam steering

Main lobe of antenna array radiation pattern can be steered by shifting the phase of signal emitted by each radiating element with respect to the antenna spacing. Phase shift provides the constructive/destructive interference to steer the beams in the desired direction. Mathematically, the phase progression can be expressed as

$$\psi_n = e^{-jkdnsin(\phi_s)}, \tag{4}$$

where d is the antenna element spacing, k is the wave vector and ϕ_s is the steering angle. Beam steering can be accomplished by changing the relative phase of antenna elements in array. Beam steered at different angles is shown in Figure 8.

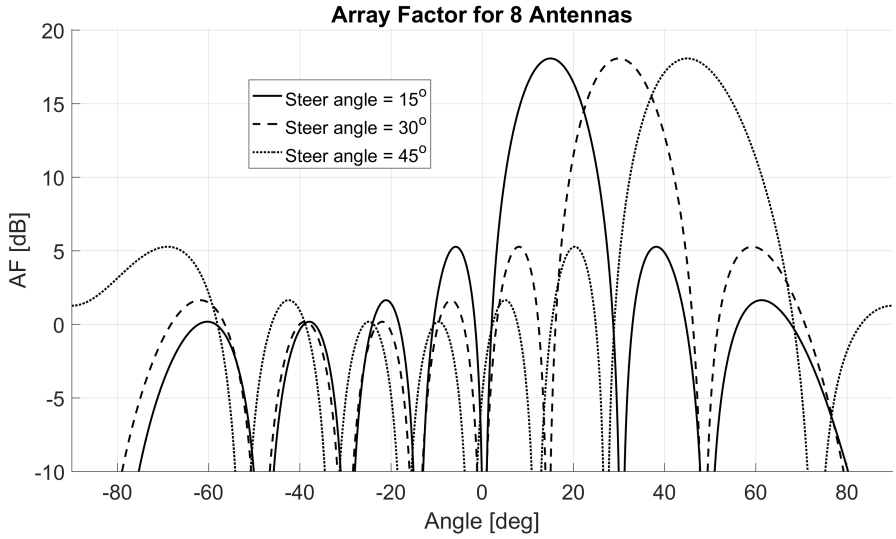

Figure 8. Beam steering at different angles.

2.3. Array figures of merit

Beamwidth, sidelobe level and maximum gain are important figures of merit (FOMs) to describe the performance of the antenna array. Beamwidth is defined as the angular separation between two identical points on opposite sides of mainlobe. Half power beamwidth (HPBW) and first null beamwidth (FNBW) are two most widely used parameters in phased arrays for radar. HPBW is the beamwidth where the mainlobe radiation power is decreased to half, and FNBW is the beamwidth between the first nulls around the mainlobe. Antenna array radiation lobes and beamwidths are shown in Figure 9.

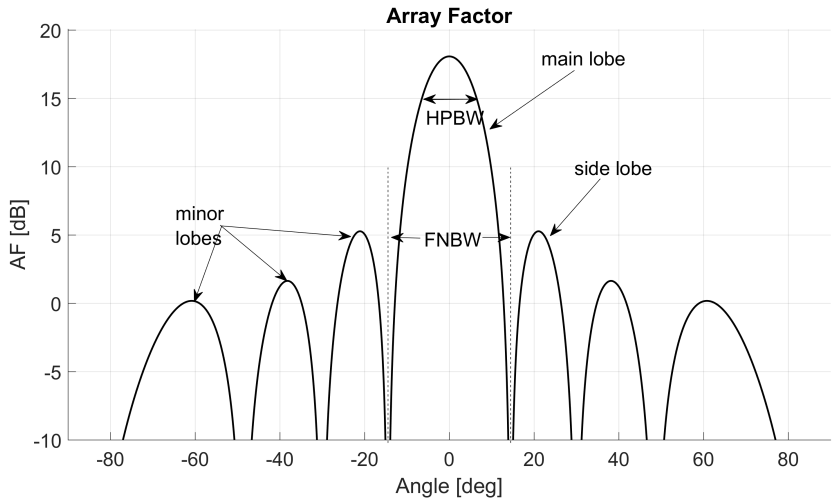

Figure 9. Antenna array radiation lobes and beamwidth.

Maximum gain or directivity describes the amount of power transmitted in the desired direction. Array gain increases with the number of elements in the array. Increasing the number of antennas in array increases the aperture size of antenna system which in turn increases gain or directivity of the array. Directivity of different number of elements is shown in Figure 10.

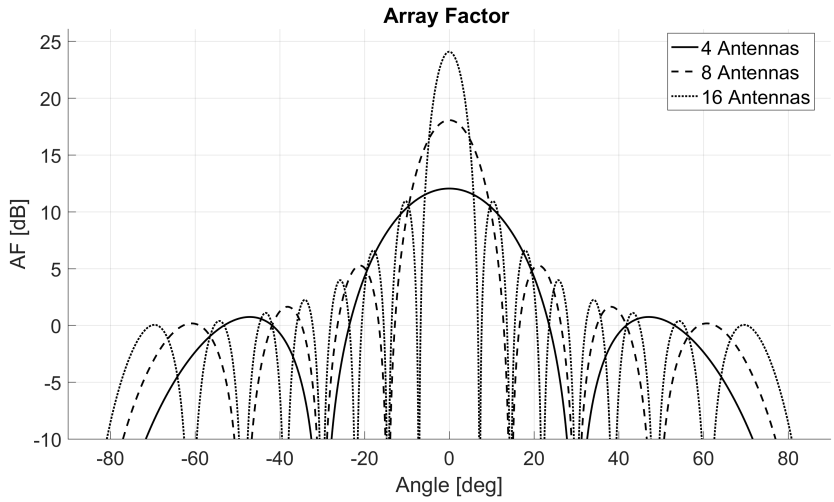

Figure 10. Directivity/gain of antenna array.

2.4. Beamforming architectures

In general, beamforming means utilization of several antennas to produce desired radiation pattern. Phase and amplitude of each antenna element are adjusted in a way that they add up constructively or destructively to a certain spatial direction or a set of directions. The two extreme beamforming architectures are analogue and digital beamforming architectures. Combining the benefits of both extremes leads to hybrid beamforming architectures.

2.4.1. Analogue beamforming

In analogue beamforming, the phase and amplitude of each antenna element is adjusted for the up-converted RF signal or intermediate frequency (IF) signal. Also local oscillator (LO) path phase shifting can be used although the solution is not very common. Either RF phase shifter or true time delays are utilized for changing the phase excitation over the antenna elements. Analogue beamforming architecture gives implementation advantages in terms of power consumption of the system and hardware complexity compared to digital beamforming architecture shown in Figure 11. Since beamforming is done in analogue front end, high performance phase shifters are required for higher frequencies. High performance phase shifters are very challenging because of higher phase and amplitude error probability. Moreover, analogue-only beamforming architecture can provide single data stream transmission from one transmitter [19].

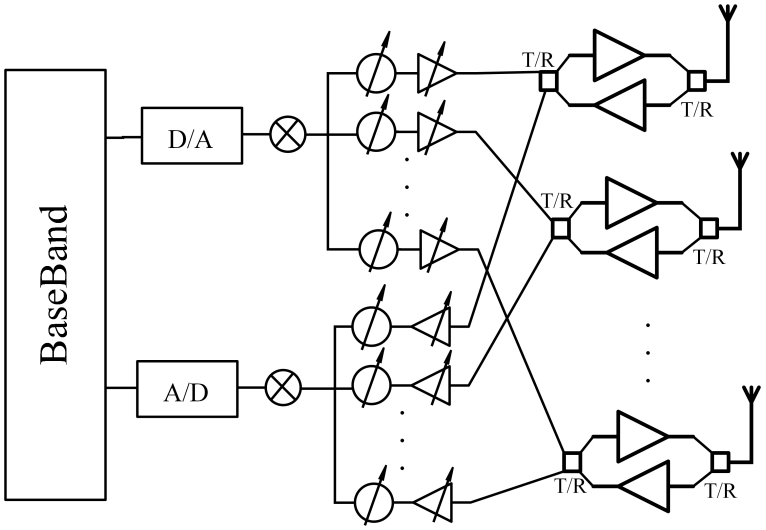

Figure 11. Analogue beamforming architecture with time-division duplex (TDD) system.

2.4.2. Digital beamforming

In digital domain, the beamforming coefficients for each antenna element are applied for the baseband signal. Hence, equivalent operation for RF amplitude scaling and phase shifting can be done in baseband by multiplication of complex numbers to have

multi-stream, multi-user connections with a variety of transmission modes. And it also provides more degrees of freedom to employ beam steering of multiple signals. However, for wideband waveforms and high data rates, one design challenge is power-hungry converters (both ADC and DAC) for each antenna separately since wider bandwidths requires high speed DAC/ADCs with high sampling rate shown in Figure 12. High power requirement increases the hardware complexity and power consumption of the system. Thus, pure digital beamforming architecture is impractical for systems utilizing high number of antennas in mmWave frequencies [19].

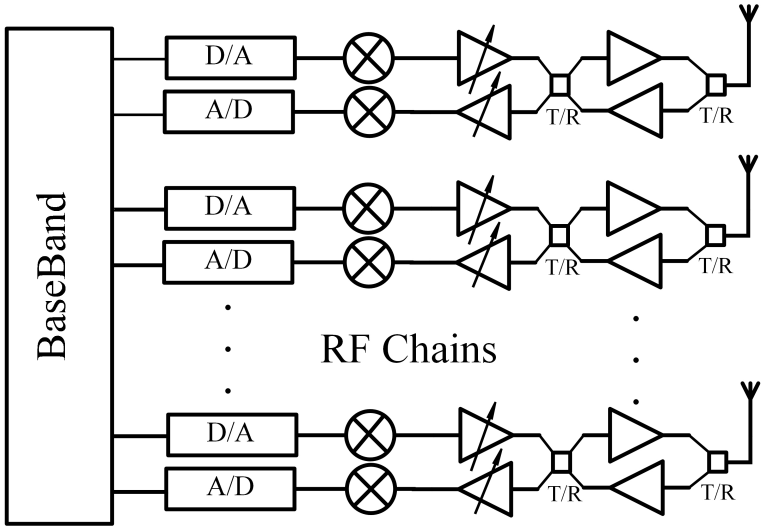

Figure 12. Digital beamforming architecture.

2.4.3. Hybrid beamforming

Hybrid beamforming combines strengths of both baseband and RF beamforming techniques. In hybrid beamforming, the processing is done in both analogue and digital domains, and it has the freedom of beamforming in several stages. Hybrid beamforming makes beam synthesis and/or hardware implementation more complex but it achieves array gain with limited number of RF chains. It also compromises on power consumption and hardware complexity [19]. Two types of hybrid beamforming architectures are mostly mentioned in the literature, which are referred to as partially connected and fully connected hybrid beamforming architecture. For each RF chain, partially connected architecture uses separate antenna array as shown in Figure 13. In fully connected architecture, the outputs from all RF chains are connected before each antenna, shown in Figure 14.

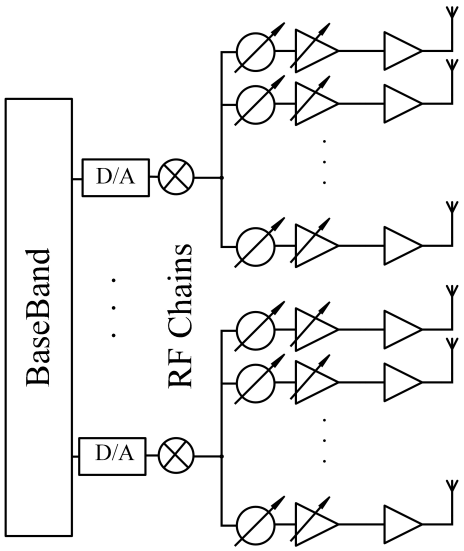

Figure 13. Partially connected hybrid beamforming architecture.

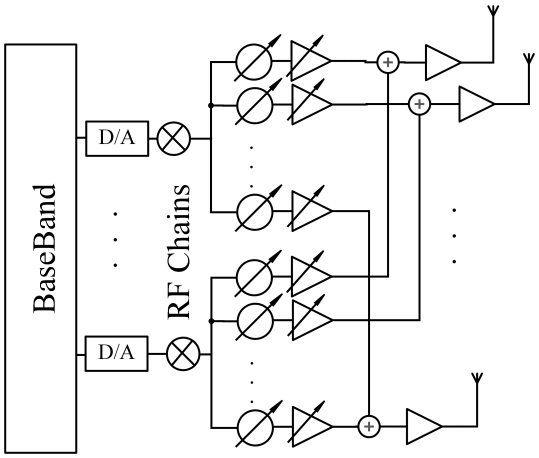

Figure 14. Fully connected hybrid beamforming architecture.

In theory, configurability of the fully connected architecture is the same as digital beamforming and better than partially connected architecture. In practice, hybrid beamforming solution can be any compromise between fully connected and partially connected architecture and hence those two only presents the two extremes of hybrid beamforming schemes. Fully connected structure increases the complexity of the system. In comparison with fully connected hybrid beamforming architecture, partially connected architecture divides the set of antennas into subarrays. Subarrays have wider beam width, less directivity, and stronger interference from other subarrays. Regardless of these problems, partially connected hybrid beamforming architecture is preferred over fully connected architecture because of circuit losses and hardware complexity present in fully connected hybrid beamforming architecture [20]. The main problem arises in fully connected architecture of the wiring of the cross-coupled RF paths. Large arrays are practically impossible to wire efficiently without unreasonable wiring losses .

3. MEMORYLESS NONLINEARITY OF RF AMPLIFIER

Power amplifiers are used in transceivers to provide gain but nonlinearity of power amplifiers distort the signals. All practical amplifiers exhibit nonlinear behaviour which becomes serious concern in modern radio communication systems, which adopt high peak-to-average-power-ratio (PAPR) waveforms to enable high data rate. Power amplifiers are required to operate in their back-off regions to meet the linearity target, while power efficiency of the PA decreases as the back-off level increases. Hence, there is always a trade-off between efficiency and linearity. Memoryless nonlinear input-output power relation of an amplifier is often described by amplitude modulation to amplitude modulation conversion (AMAM) and amplitude modulation to phase modulation conversion (AMPM) of the amplifier. Other merits which describe the performance and nonlinearity of PA are also discussed. Mathematically, nonlinearity of PA is modelled by Taylor and envelope power series in this chapter. For the sake of simplicity, memory effects impacting to PA non-linearity are neglected from the analysis in this thesis.

3.1. RF power amplifier

In general, purpose of an amplifier is to amplify signal, i.e. multiply it with a certain scalar value. Ideal amplifiers are linear and operate only in linear region. However, all amplifiers are nonlinear in practice. Nonlinear amplifier operates in three different operating regions, which are cut off, linear and saturation regions, depending on the input drive level and biasing of the transistor as shown in Figure 15. When input signal is low, amplifier is operating in cut off or weakly non-linear region and output has exponential form. In linear region, amplifier performs as ideal amplifier until input rises high enough, so that output saturates to the maximum output level. In saturation region, nonlinear amplifier smoothly decreases amplitude of the output signal [21].

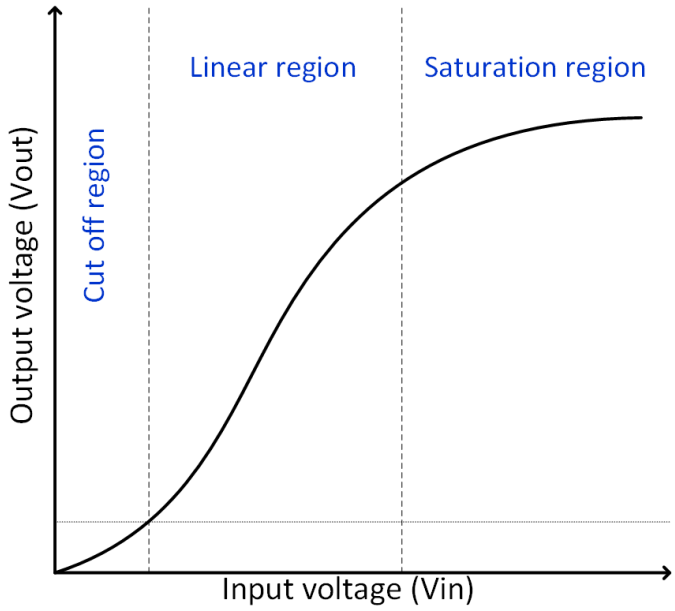

Figure 15. Operating regions of nonlinear amplifier.

The operating point of PA is called quiescent point (Q-point). It is steady-state direct current (DC)-voltage or -current at the collector or drain of the transistor when there is no input signal. Different PA classes have different Q-points. Power amplifiers are divided into classes by the conduction angle of the collector current of the transistor. Different classes have different characteristics in terms of efficiency and linearity. Class A amplifier is biased in a way that the output current flows all the time. DC-power is constant and theoretical efficiency of class-A power amplifier is at maximum 50%. Conduction angle of a class B is approximately 180^o. However class B amplifier is significantly less linear than class A amplifier. Class AB amplifier is a compromise between Class A and Class B in terms of efficiency and linearity. For a sine-wave signal, class AB amplifier conducts between 180^o and 360^o and has efficiency between 50% and 78.5%. Class C amplifier has conduction angle of less than 180^o and has poor linearity. Other amplifier classes are used for switching purposes [22]. Classes D to T have very high efficiency [22]. Classes of amplifier with different efficiencies are shown in Figure 16.

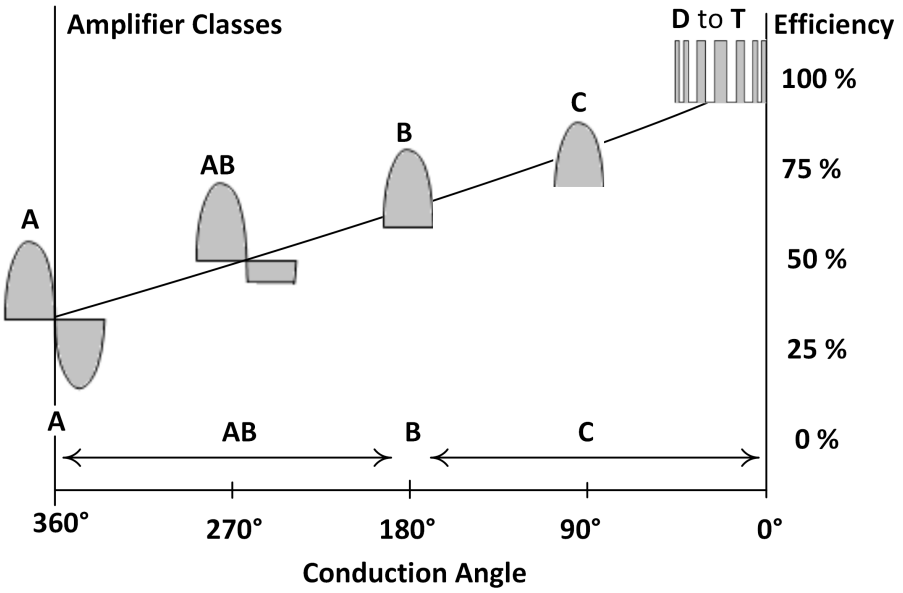

Figure 16. Conduction angle and achievable efficiencies of RF PAs [22].

Power-added efficiency (PAE) is a commonly used FOM for rating the efficiency of a power amplifier while taking into account the gain of the amplifier. PAE is different than power or drain efficiency. Drain efficiency is the ratio of output RF power to the input DC power. Drain efficiency is a measure of how much DC power is converted to RF power, for a single device. Power efficiency is simply a ratio of output signal power to the DC power but PAE is ratio of difference of the output and input signal power to the DC power. DC power which is not converted to RF output power, dissipates in the form of heat. If P_{OUT} is the output signal power, P_{IN} is the input signal power and P_{DC} is the DC power supplied to the power amplifier, then PAE can be mathematically expressed as

$$PAE = \frac{P_{OUT} - P_{IN}}{P_{DC}}. \tag{5}$$

Intercept point is the common measure of distortion of an amplifier at a given operating point. Theoretically, the power level at which the power of the desired tone and the nth-order intermodulation products intersect at backoff (from the intercept point). The higher the output at the intercept, the better the linearity and the lower the IMD. The IP3 value essentially indicates how large signal the amplifier can process before IMD occurs [23]. 1 dB compression point is defined as power level at which the signal output is already compressed by 1 dB, shown in Figure 17.

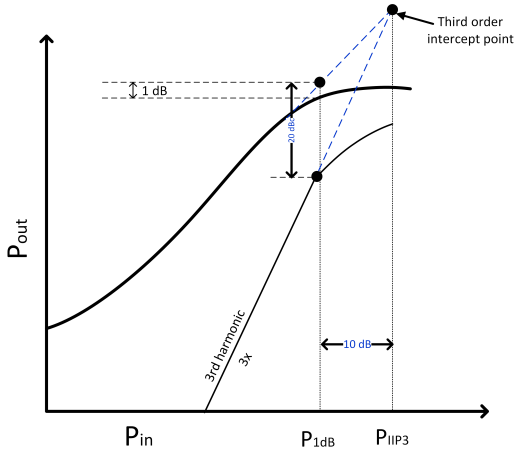

Figure 17. Illustration of intercept points and 1dB compression point.

3.2. AMAM / AMPM

Wireless systems encode the information in both amplitude and phase of the RF signal to increase the data rate and encoding of the signal is baseband process. Baseband signal is first up-converted, then amplified by power amplifier. PA nonlinearity distorts the amplitude and phase of the output signal causing amplitude and phase errors. This degrades the performance of the system. AMAM and AMPM measurements are consisted of acquiring the input-output relations of the PAs in both amplitude and phase. Nonlinearities of amplifiers are often described by the amplitude transfer characteristics AMAM and phase transfer characteristics AMPM shown in Figure 18.

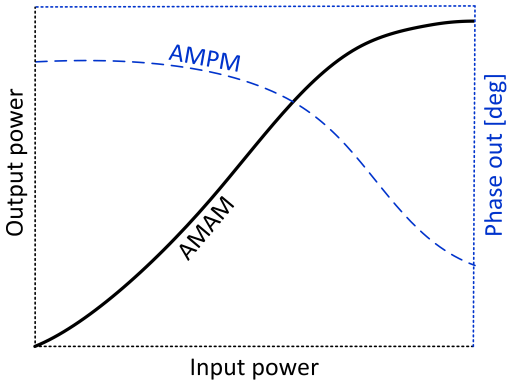

Figure 18. AMAM / AMPM.

3.3. Inter-modulation and harmonic distortion

When an amplifier is operating in non-linear region, it produces harmonics of the amplified inputs. Harmonics generated at the output are integer multiples of the fundamental input frequencies. The harmonics are usually outside of the amplifier bandwidth, so they can be potentially filtered away. However, non-linearity will also produce a mixing effect of two or more signals. If the signals are relatively close to each other in frequency, the sum and the difference of frequencies called intermodulation products can occur within or close to the desired signal band. These distortion terms cannot be filtered out and hence they will ultimately become become interference for the desired signal, as well as for other systems operating at frequency bands nearby. Harmonics and intermodulation products for two-tone input are shown in Figure 19.

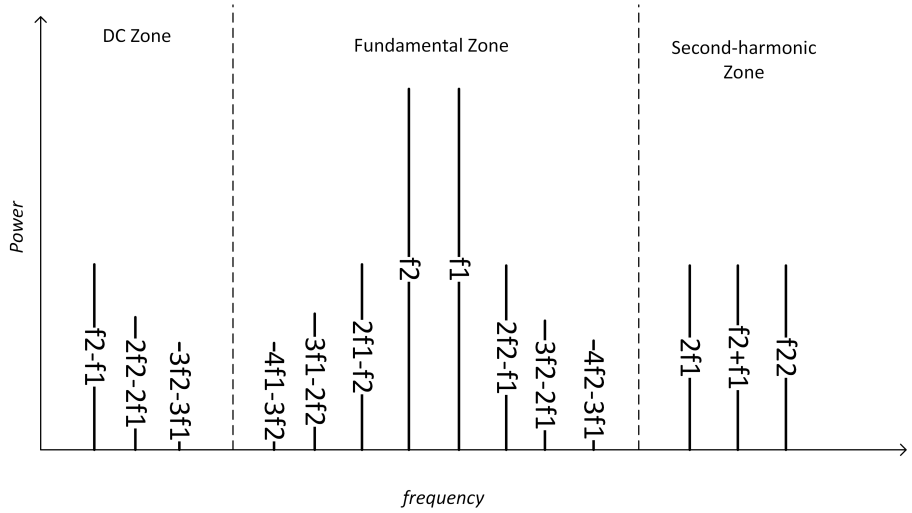

Figure 19. Harmonics and intermodulation products for two-tone input.

3.4. Nonlinearity with modulated and multicarrier signals

Modulated waveform has usually time-varying envelope which increases the dynamics of the signal. PAPR is a measure of the dynamics of the waveform. Multi-carrier signals with modulated waveform have high PAPR, which requires higher linearity of PA. If P_{PEAK} is the peak power and P_{AVG} is the average power, then PAPR can be calculated as

$$PAPR = \frac{P_{PEAK}}{P_{AVG}}. \tag{6}$$

Spectral regrowth at the PA output is caused by the nonlinearity of the amplifier. Because of intermodulation, spectrum of assigned channel spreads over the channel of interest and causes unwanted interference to adjacent channels. Adjacent channel power ratio (ACPR) is the ratio of total output power measured to the total power integrated in the adjacent channel bands. In other words, degree of signal spreading into adjacent channel, is caused the nonlinearities of the PA as shown in Figure 20. ACLRu signifies

that power from the main channel is leaked into the channel above. ACLRl stands for that power from the main channel is leaked into the channel below.

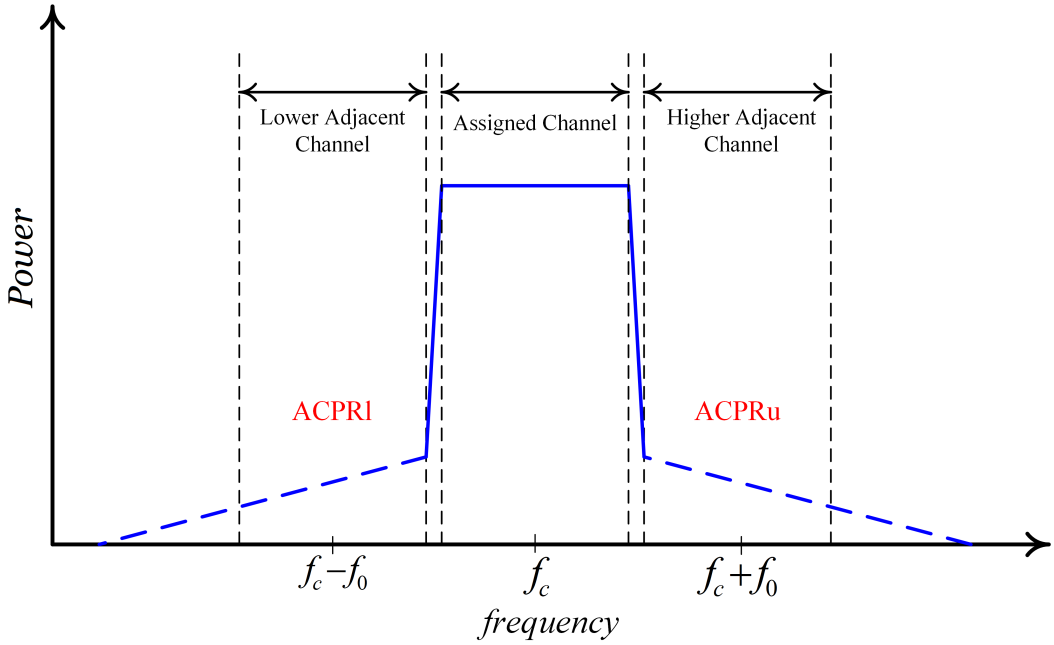

Figure 20. Spectral regrowth caused by the nonlinearity for a communication signal.

Multitone intermodulation ratio (MIMR) is the ratio of the common fundamental power-per-tone to the power of the distortion component present in the lower or upper adjacent bands. It is the measure of the effects of nonlinearity on a multicarrier signal, as the ratio between the wanted signal tone power and the highest intermodulation tone power just outside of the wanted band [24], shown in Figure 21.

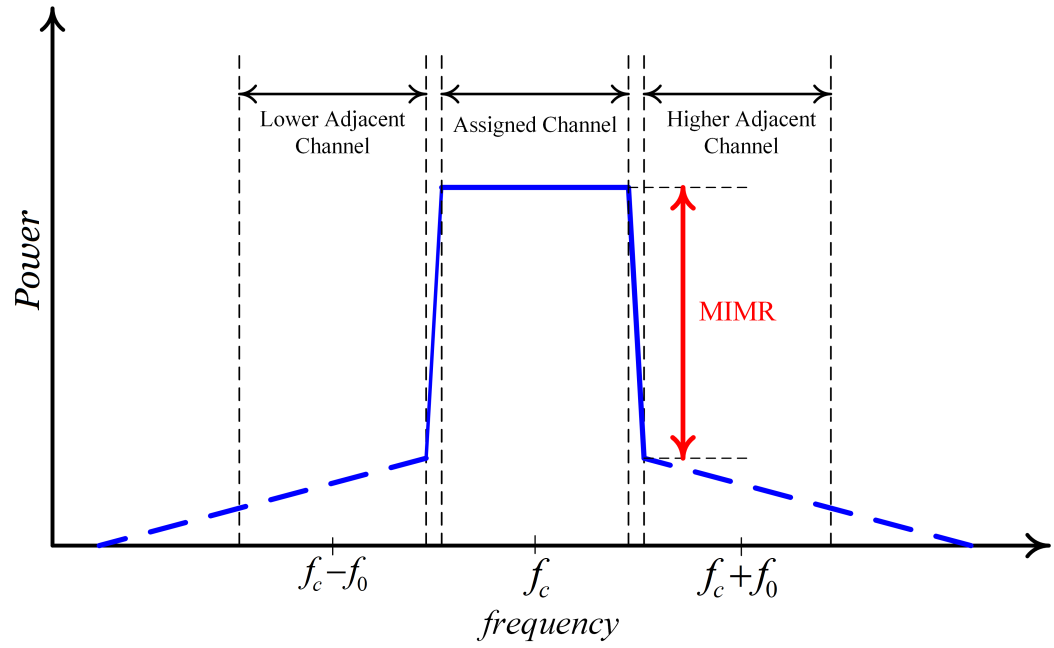

Figure 21. Multitone intermodulation ratio.

In-band performance of a transmitter or a receiver can also be measured by error vector magnitude (EVM). EVM is a measure of modulation quality and error performance. EVM is a function of both noise and distortion. EVM specifications require improved PA linearity, typically a PA is required to have less than 3% EVM at rated power [25]. EVM is the ratio of the power of the error vector to the root mean square (RMS) power of the reference signal shown in Figure 22. If A_{error} is RMS amplitude of error vector and $A_{reference}$ is RMS amplitude of reference signal then EVM in dB can be mathematically calculated as

$$EVM_{dB} = 20\log_{10}(A_{error}/A_{reference}) \tag{7}$$

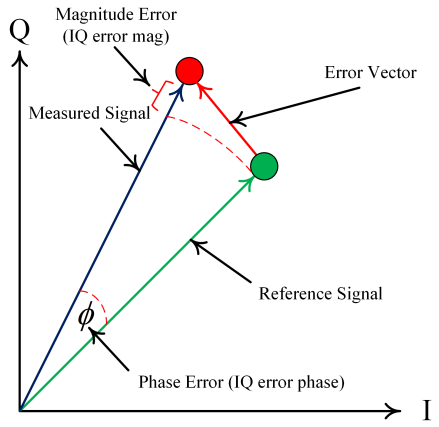

Figure 22. Error vector magnitude and phase.

EVM is also related to the signal-to-noise ratio (SNR) and signal-to-distortion ratio (SDR). SNR and EVM relation [26] can be mathematically written as

$$\text{EVM}_{\text{RMS}} = (\frac{1}{SNR})^{1/2}. \tag{8}$$

Higher SNR means better quality of signal. When the levels of the noise and distortion are smaller, probability of having an error in the data is consequently smaller. In addition, modulation scheme is related to error probability. Higher modulation schemes can be used when error probability is lower. Moreover, higher modulation scheme means higher spectral efficiency (bits/s/Hz) within the same bandwidth and hence tighter EVM requirement. Examples of the system EVM requirements for different modulation schemes are given in Table 1 [27].

Table 1. EVM specification.

Modulation Scheme	Required EVM[%]
QPSK	17.5%
16 QAM	12.5%
64 QAM	8%
256 QAM	2.2%

3.5. Modelling of PA nonlinearity

Modelling of RF PA is very intense research topic. RF PA is linear if the output power of PA is a constant multiplied by the input power of the amplifier. Practical amplifiers are nonlinear. The nonlinear output V_{out} of memoryless amplifier can be modelled mathematically by Taylor series as

$$V_{out}(t) = V_{out(DC)}+a_1(V_{in})+a_2(V_{in})^2+a_3(V_{in})^3+a_4(V_{in})^4+a_5(V_{in})^5+\cdots+a_n(V_{in})^n, \tag{9}$$

where $V_{out(DC)}$ is the DC-component of the output signal, V_{in} in the input signal power. a_1 is the linear gain coefficient, and a_2, a_3,...a_n are coefficients for 2,3,...n order nonlinearity contributors. Even-order nonlinearity leaves the fundamental signal frequencies unchanged, but produces harmonic components at even multiples of the fundamental signal frequencies upto the order of the nonlinearity. Even-order nonlinearity can be mitigated by filtering. Odd-order nonlinearity produces harmonics at odd multiples of fundamental signal frequencies upto the order of the nonlinearity. Odd-order nonlinearity causes change in the gain of fundamental signal frequencies and lower order intermodulation distortion. However, non-linearity will also produce a mixing effect of two or more signals, which fall in the channel bandwidth and cannot be filtered out, and distort the signal [28]. In this thesis, nonlinearity is taken up to third-order for ease of understanding the behaviour of intermodulation distortion in beamfomring system. Memoryless amplifier is also modelled by envelope power series and mathematically expressed as [29]

$$v_{out}(t) = \sum_{k:=odd}^{\substack{N_p \\ k=1}} b_k|v_{in}(t)|^{k-1}v_{in}(t), \tag{10}$$

$v_{in}(t)$ and $v_{out}(t)$ are the instantaneous complex envelopes of the input and output waveform, respectively. N_p is the is order of polynomial and k is the order of the nonlinearity term. The main difference in Taylor and envelope power series model is that Taylor model includes all the frequency components, and V_{in} and a_i are real-valued but in envelope power series model, it only covers the fundamental band and signals, also the coefficients are complex. Throughout the rest of the thesis, envelope power series is used a PA model with specific coefficients described in the previous chapters.

4. MEASUREMENT TECHNIQUES FOR CHARACTERIZING NONLINEARITY IN MULTIANTENNA TRANSMITTER

AMAM, AMPM, two-tone and multi-tone tests are well-known techniques to characterize the nonlinearity of power amplifier. For the beamforming transmitter, where each RF branch has individual sources of PA nonlinearity when operating together, the concept of IMD must be revised to understand how these should be characterized and specified. In this chapter, measurement techniques are used to measure amplitude and phase of the intermodulation terms. IMD measurements describe the power ratio between the power level of fundamental tones and third-order distortion terms. Phase information of IMD components is important in beamforming systems where progressive phase makes the beam of nonlinearity and hence it is measured in this chapter.

4.1. AMAM and AMPM measurements

AMAM in Figure 23 is the measured output amplitude versus input amplitude (Example is measured from ZFL-500LN Amplifier [30]). AMPM in Figure 24 is the measured output phase versus the input amplitude. In these measurements, single frequency is fed into the PA and its power is swept to achieve compression at the amplifier output. AMAM and AMPM are good measures to illustrate the output power and phase behaviour of an amplifier.

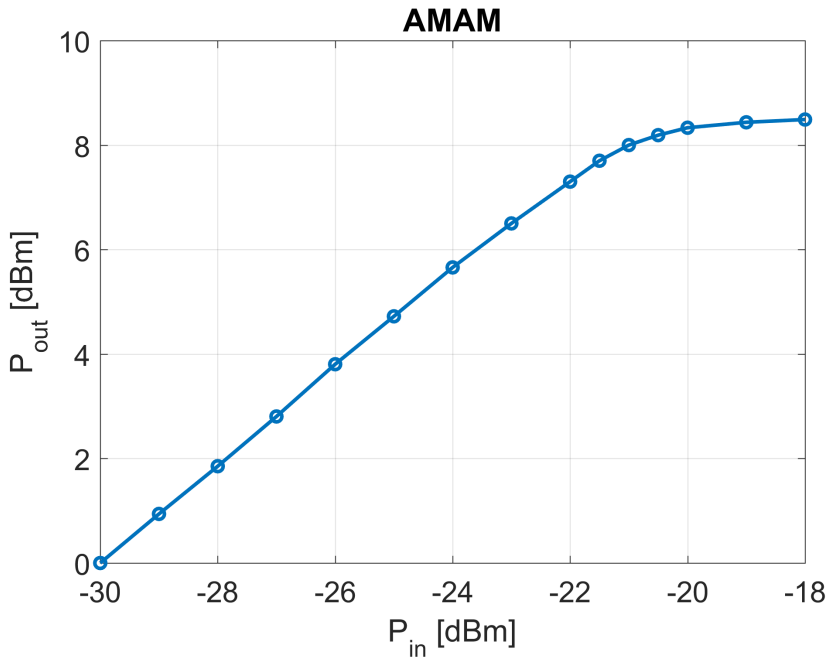

Figure 23. Measured AMAM.

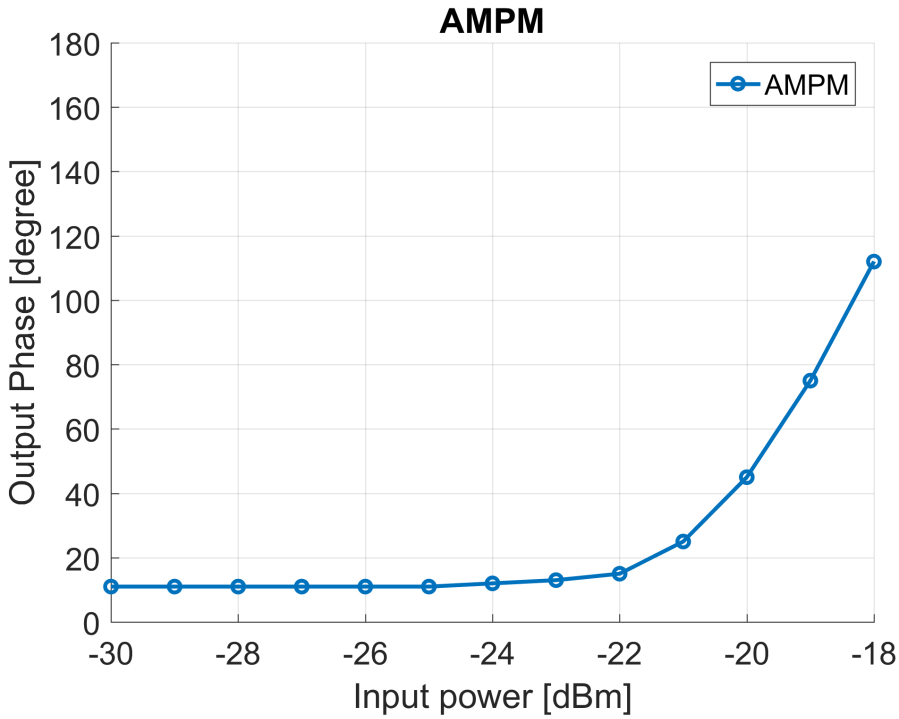

Figure 24. Measured AMPM.

4.2. Two-tone test

In two-tone test, a signal comprised of two tones is fed into power amplifier and intermodulation products are measured in band. Nonlinear behaviour of the PA produces a mixing effects of two tones, which are lower intermodualtion term at frequency $2f_1 - f_2$ and higher intermodualtion term at frequency $2f_2 - f_1$. Two-tone test is discussed in previous chapter and shown in Figure 25 below.

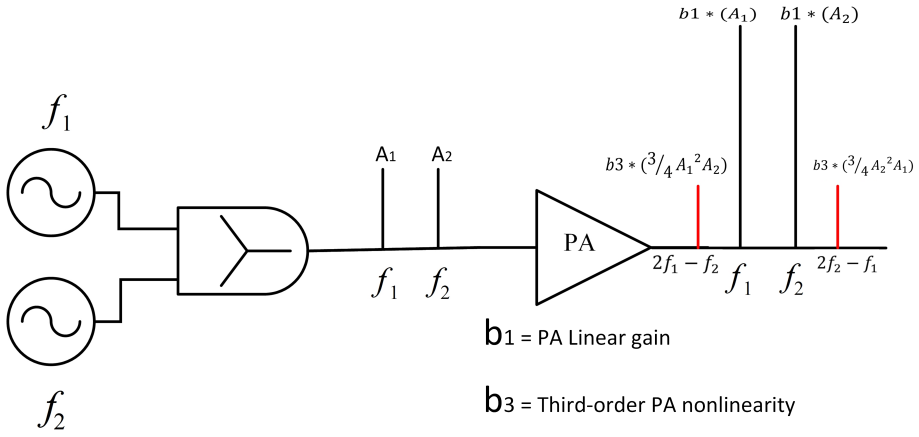

Figure 25. Two-tone test.

4.3. Characterizing IMD amplitude and phase

Intermodulation terms depend on the phase and the amplitude of the fundamental tones, which is measured in this chapter to validate the simulation model used in the next chapter. Measurement setup presented in Figure 26 illustrates amplitude and phase of fundamental two tones and their intermodulation terms. Concept of the setup is that when two signals with same frequency and same amplitude and opposite phase are summed, they cancel each other. In this technique, the two tones (f_1 and f_2) are generated from the signal generator 1 and 2, respectively. These two tones are combined before the PA. Third signal generator is combined at the output of the amplifier.

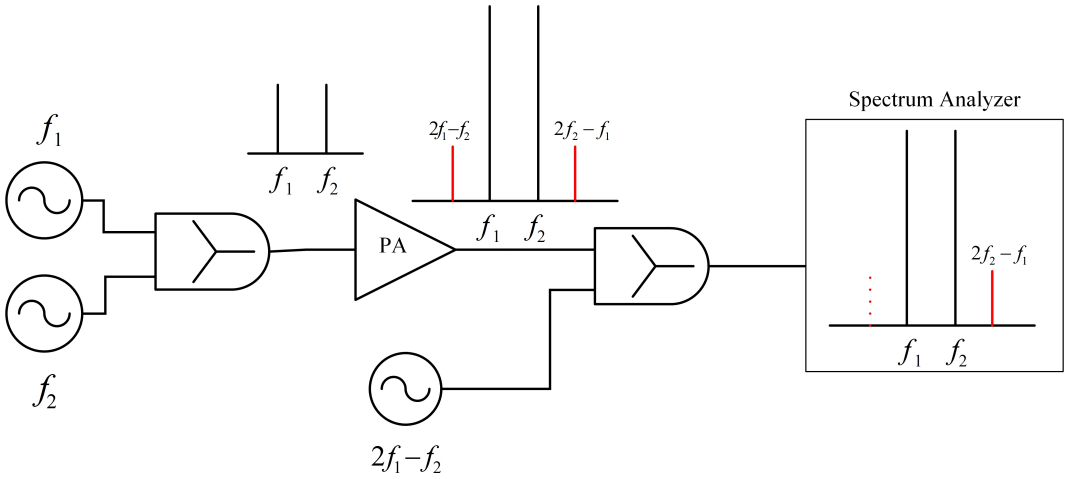

Figure 26. Measurement Setup.

Third signal generator produces the tone at same frequency and power as lower intermodulation term, tone 1, tone 2 and higher intermodualtion term one by one. Phase of the signal generator is adjustable and the Matlab code to control the phase is attached in Appendix 8.1. Sweeping the phase of third signal generator will cancel the tone due to destructive interference. Phase of third signal generator, which cancels out the tone is 180 degree shifted phase of respective tone.
Deducting 180 degree phase from the cancelling phase of third signal generator gives the phase of respective tone. When measurements are taken, there are certain issues which are needed to be taken into consideration for the accuracy of the measurement results. Combiners and cables used in the setups add phase and amplitude offset. Different frequencies passing through the same length cable have different output phases due to different wavelengths. Instruments (esp. signal generators) involved in measurement setup should have common frequency reference (frequency standard). Otherwise if multiple instruments with different frequency references are used, it may lead to frequency or phase error.
When frequency of the signal generator is changed, Voltage Controlled Oscillator (VCO) takes a little time to lock the phase of new frequency with phase of reference frequency. Phase measurements taken during that time might be incorrect. Thus, signal generator should be given enough time to settle. If the signal generator is not given enough time to settle after changing the frequency, it might lead into considerable problems. Handling the setup devices in such a manner that they create accurate

and precise results is challenging. To facilitate the process, all the measurements are completely automatized. Devices are set up using SCPI commands from Matlab script via general-purpose interface bus (GPIB) device. Matlab script is attached in Appendix 8.1. Theoretically, phase of lower intermodulation term $(2f_1 - f_2)$ is $2\theta_1 - \theta_2$ and phase of higher intermodulation term $(2f_2 - f_1)$ is $2\theta_2 - \theta_1$ as calculated mathematically in the previous chapter. By changing the phases of tones at PA input will change the phase of IMD terms at PA output. We sweep the phase of signal generator 2 (tone 2) at PA input while keeping the phase of signal generator 1 (tone 1) as zero and measure the phase dependence relationship of IMD terms and input tones. Devices and instruments used in measurements are given in Table 2. Block diagram of measurement setup and flow diagram of Matlab script are given in Figure 27 and Figure 28.

Table 2. Measurement devices/instruments.

Instrument/Device	Model
Signal Generators	Marconi 2024
Amplifier	ZFL-500LN
Spectrum Analyzer	R&S (FSIQ 7)
PA Power Supply	EA-3025S
GPIB	NI (GPIB-USB-HS)
GPIB connector	IEEE-488
Interface/Software	Matlab 9 (R2016a)

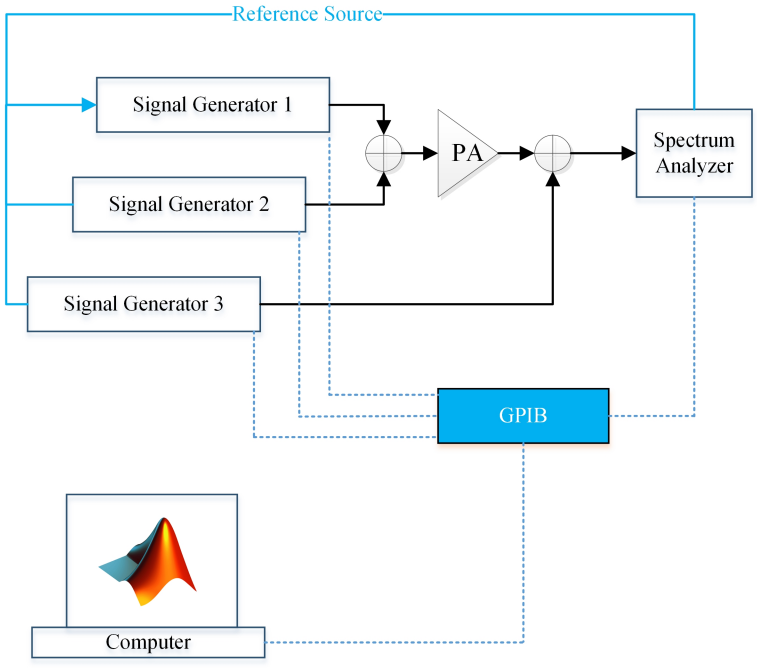

Figure 27. Block diagram of measurement setup.

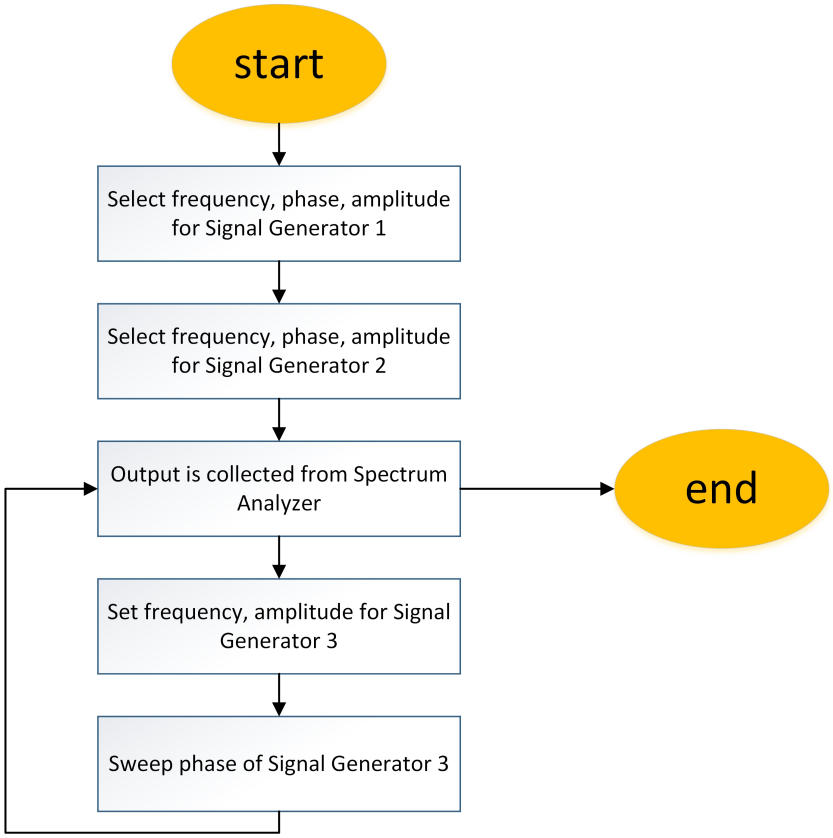

Figure 28. Matlab script flow chart.

First, we measure the phase of tone 1 by setting up the frequency of signal generator 3 equivalent to the tone 1 frequency. Amplitude of signal generator 3 is set to be exact amplitude of tone 1. In case of difference of power levels of tone 1 and signal generator 3, tone 1 will not be cancelled completely. We sweep the phase of the signal generator 3 and find the phase where it cancels the tone 1 completely shown in Figure 29. This cancelling phase has negative phase compared to phase of tone 1. By subtracting 180 degree from the phase of the third signal which is providing the cancellation, we get the phase of tone 1. Phase offset occurs in the results due to passive components used in the setup. Additionally, the cables used in the setup produces phase offset. Different frequencies passing same length cables have different phases at output because of different wavelengths, which is seen as phase offset in the results. Phase of f_2 is changing at the input of amplifier and is measured at output of amplifier given in Figure 30, which shows that it changes accordingly. Figure 31 presents the same measurement for lower IMD and Figure 32 to the higher IMD, respectively. Measurement results verify the theory of phase relationship of IMD components with fundamental tones. $\Delta\phi$ is the phase difference between fundamental two-tone.

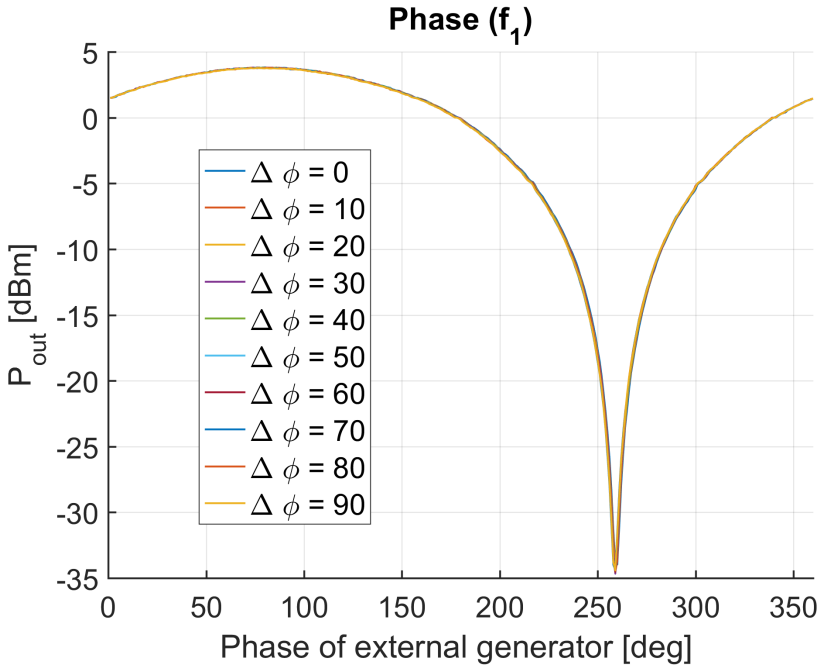

Figure 29. Phase between two-tone vs Phase of f_1.

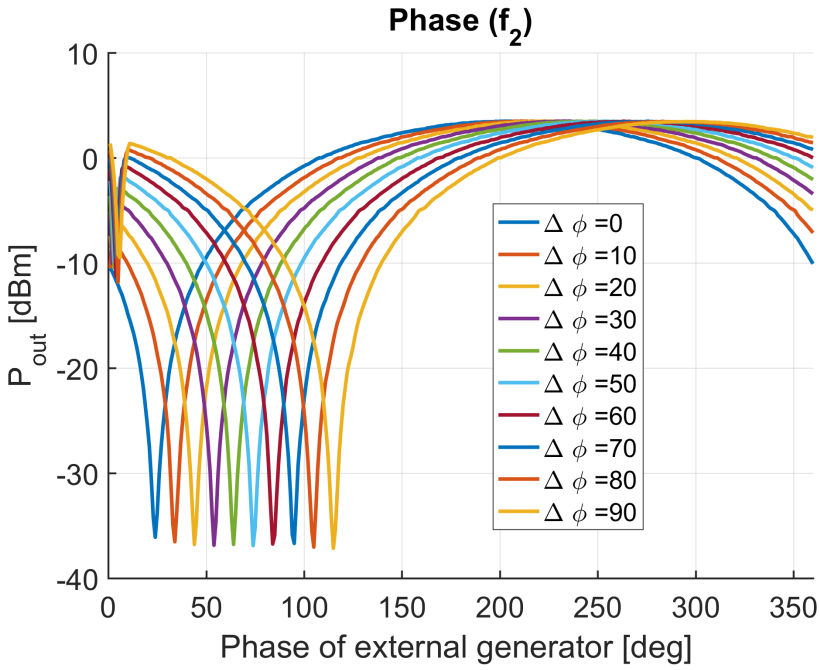

Figure 30. Phase between two-tone vs Phase of f_2.

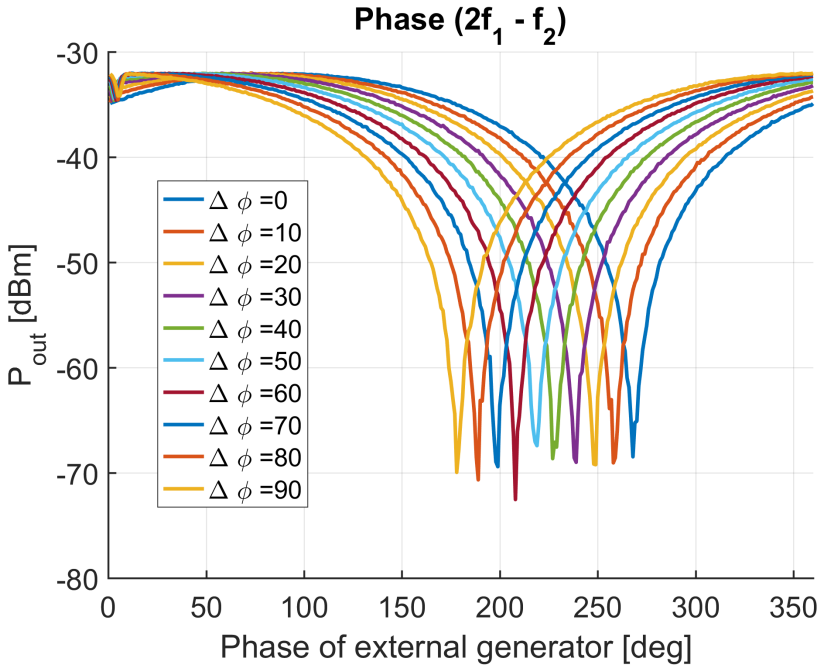

Figure 31. Phase between two-tone vs Phase of IMD_L.

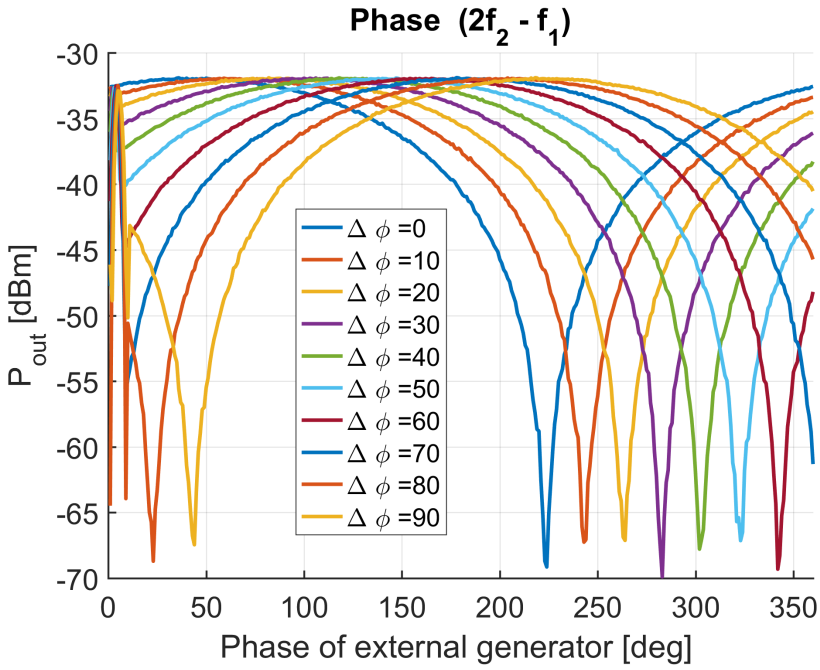

Figure 32. Phase between two-tone vs Phase of IMD_H.

Figure 33 presents the output phase change of amplifier with respect to the change of the amplifier input phase by combining the measurements results. Phase offset due to the passive components remains same for one frequency but phase offset changes when signal generator switches from one frequency to another. Measurement results without offset are shown in Figure 34 along with illustrating that the phase of lower

intermodualtion term varies as $2\theta_1 - \theta_2$ and phase of higher intermodualtion term varies as $2\theta_2 - \theta_1$.

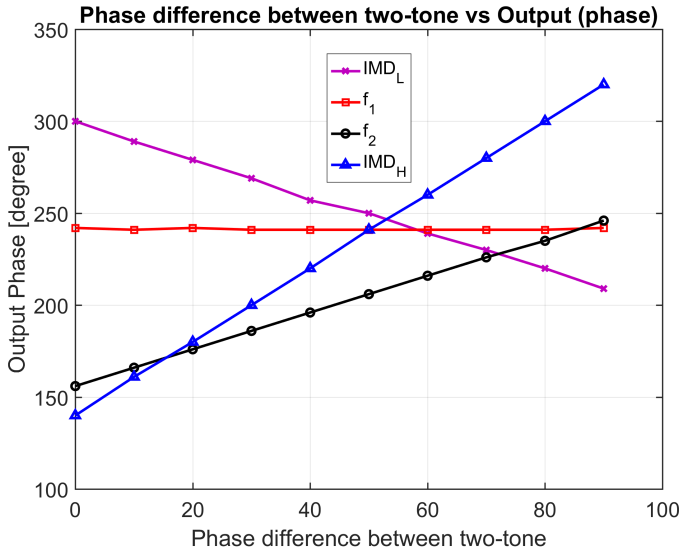

Figure 33. Phase difference between two-tone and output phase.

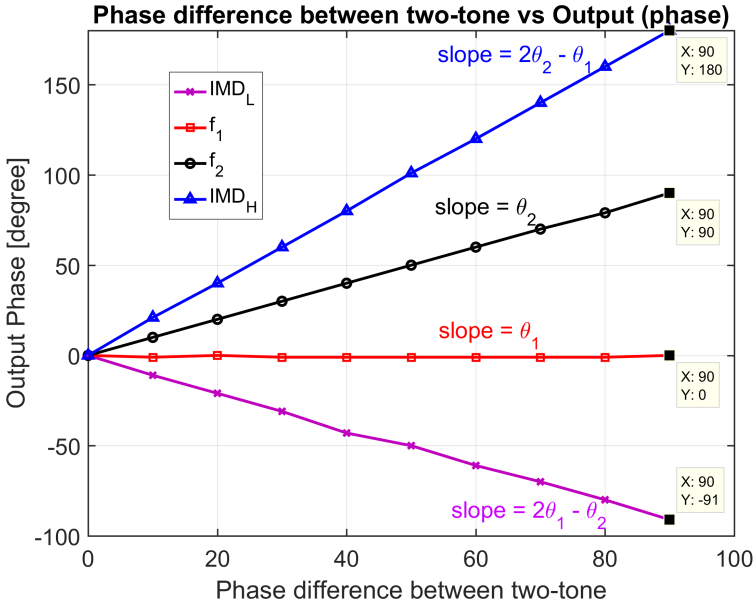

Figure 34. Phase difference between two-tone and output phase.

Measurement results indicate that the phase of the IMD components is dependent on the input signal phase. Recognition of this dependence is essential in beamforming because steering the beam requires of changing input signal phase progression over the antennas, which causes changes in the phase of IMD components. In case the IMD terms are directed in same direction as main beam, IMD degrades the SNR of the beam for the modulated signal; in case IMD are directed in other directions than the main beam, it may lead to change in sidelobe level of the rms-beam. Effects of IMD in beamforming scenarios are simulated in the next chapter.

5. EFFECTS OF PA NONLINEARITY IN A BEAMFORMING SYSTEM

Antenna array is an efficient solution to combine signals over-the-air. PA nonlinearity impairs with the transmitted signal and is also combined over-the-air. Out-off-band distortion causes spectral spreading of the transmitted signal in terms of higher and lower ACPR. In-band distortion causes amplitude and phase errors in the transmitted signal and beamforming coefficients. In other words, amplifier distortion can also be seen as generation of new frequency components either as harmonics or intermodulation components of the original signal in frequency domain. Nonlinear amplifier distortion over-the-air degrades the overall beam pattern and performance of the system. This chapter simulates and discusses the effects of nonlinear PA distortion in the array far-field in single-beam and multibeam scenarios.

5.1. Power amplifier modelling

PA is modelled in Matlab by least square estimation of polynomial coefficients. PA modelled by third-order polynomial is shown in Figure 35. It is good fitting by third-order polynomial unless PA is driven in the deep compression shown in Figure 36. Deeper into the compression, more coefficients are required to model the PA behavior accurately. Also, higher order polynomial models better the desired response but on the other hand it is more complex. In deep compression, impact of higher order distortion is important, therefore those should be taken into account to model the PA response accurately. Figure 37, 38 and 39 illustrate the higher order polynomials. Furthermore, the used models neglects the memory effects of the amplifier which are known to be an issue especially with the wideband signals.

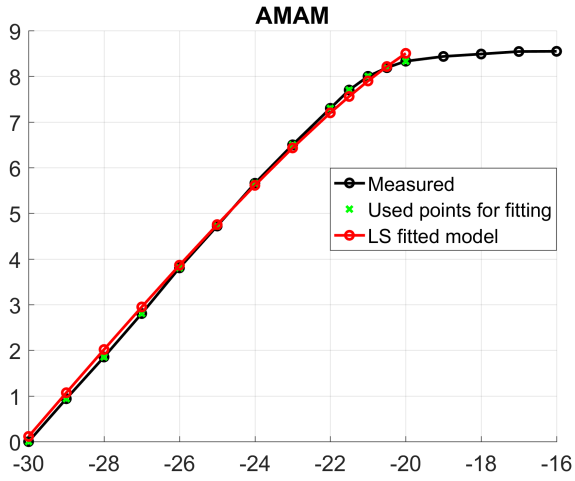

Figure 35. PA modelled by third-order polynomial.

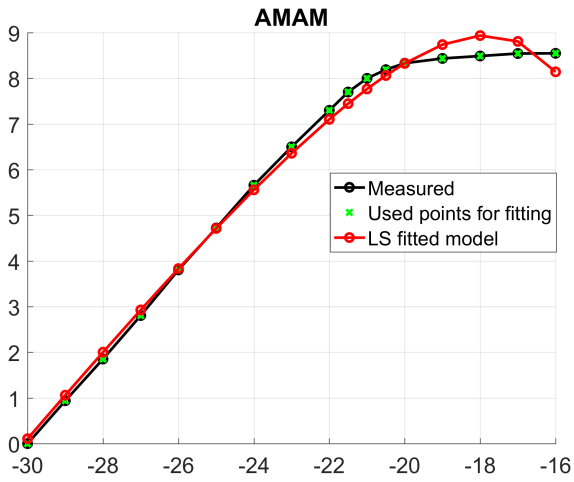

Figure 36. PA modelled in deep compression by third-order polynomial.

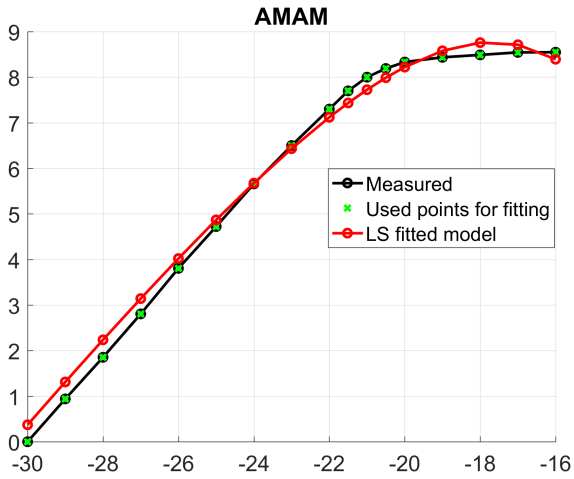

Figure 37. PA modelled in deep compression by fifth-order polynomial.

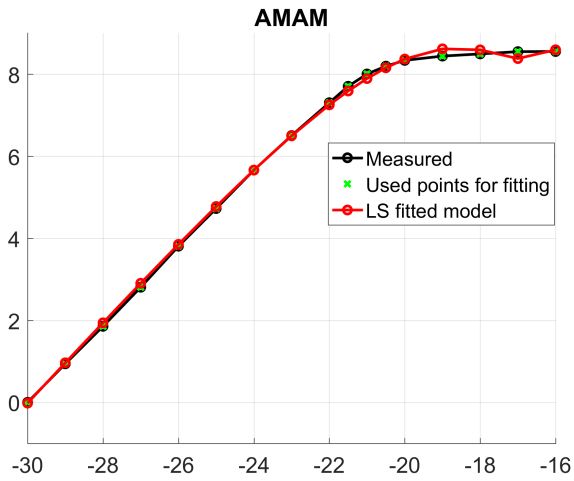

Figure 38. PA modelled in deep compression by seventh-order polynomial.

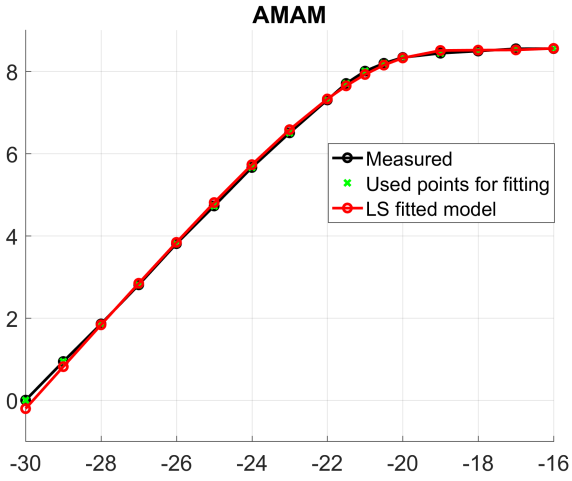

Figure 39. PA modelled in deep compression by ninth-order polynomial.

5.2. Intermodulation in single-beam transmission

In order to analyze the effects of PA nonlinearity in single-beam transmission, two-tone signal is used as common input for all parallel antenna paths in a phased array transmitter. The system model for the test is presented Figure 40. X_{array} is the modelled input two-tone signal with amplitude A_{tones} given in equation (11), where $\triangle f$ is frequency spacing between two tones and δ is Dirac delta function. X_n is input to the PA_n and w_n is the beamformer coefficient of antenna n.

$$X_{array} = A_{tones}[\delta(f_c - \triangle f/2) + \delta(f_c + \triangle f/2)], \tag{11}$$

$$X_n = w_n X_{array}, \tag{12}$$

$$w_n = g_n e^{j\phi_n}. \tag{13}$$

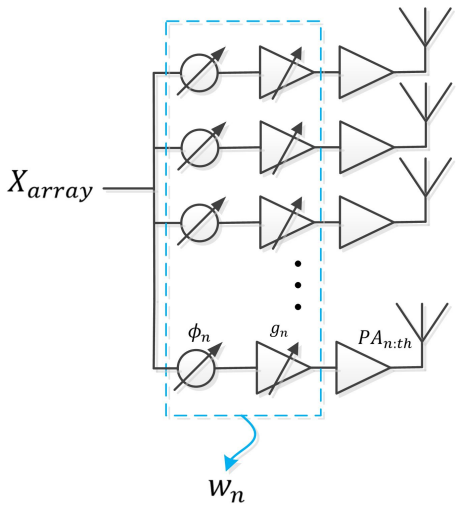

Figure 40. System model for a two tones/single-beam test.

Beamformer coefficients are defined by the phase shifter ϕ_n and variable gain amplifier g_n. Polynomial model of nonlinear amplifier is modelled in frequency domain as

$$\begin{aligned} f_{PA_n}(X(f)) = b_{n1}X(f) + b_{n3}X(f) * X^*(f) * X(f) \\ + b_{n5}X(f) * X^*(f) * X(f) * X^*(f) * X(f) \\ + b_{nN} \cdots + X(f)X(f)^* \ldots X(f), \end{aligned} \tag{14}$$

where b_{n1} is the gain of the nth amplifier, b_{n3} is third-order, b_{n5} is fifth-order nonlinear terms of n_{th} PA and b_{nN} is n:th-order nonlinear terms of n_{th} PA respectively. Input two-tone signal convolves with PA response in frequency domain and amplifier nonlinearity causes generation of unwanted new frequency components in-band given in Table 3 and frequency response of the PA output is shown in Figure 41

Table 3. In-band 3^{rd} order nonlinear terms (two-tone)

Index	**Frequency**	**Phase**
Term 1	$(2f_1 - f_2)$	$(2\theta_1 - \theta_2)$
Term 2	f_1	θ_1
Term 3	f_2	θ_2
Term 4	$(2f_2 - f_1)$	$(2\theta_2 - \theta_1)$

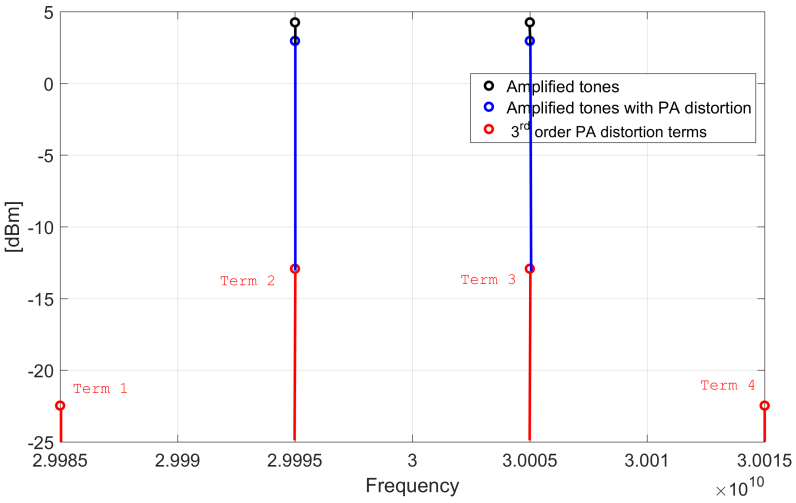

Figure 41. In-band 3^{rd} order nonlinear terms (two-tone)

These intermodulation terms are also beamformed and transmitted over-the-air, which combines and impairs the main beam and degrades SNR of the beam. Array factor is modelled in Matlab to demonstrate the beam pattern and nonlinearity effects on beam pattern. Array modelling was studied in Chapter 2 given in equation 16 and y_n is the beamforming coefficient of the n_{th} antenna given as

$$\begin{aligned} y_n &= f_{PA_n}(X_n) \\ &= f_{PA_n}(w_n X_{array}) \\ &= f_{PA_n}(w_n A_{tones}[\delta(f_c - \triangle f/2) + \delta(f_c + \triangle f/2)], \end{aligned} \tag{15}$$

$$AF(\theta, \phi, f) = \sum_{n=1}^{N} y_n e^{j2\pi f(n-1)d(sin(\theta)cos(\phi)}. \quad (16)$$

Phase of intermodulation is dependent on the phase of fundamental tones which has been measured in the previous chapter. Fundamental tones and intermodulation products are beamformed by the antenna system and transmitted over-the-air by the beamforming system. Intermodulation terms which have the same phase and frequency as the fundamental tones (Term 2 and Term 3) falls in the useful beam direction and causes gain compression. Intermodulation terms (Term 1 and Term 4) have different frequencies and different phase from the fundamental tones and they could potentially fall into different directions than the useful beam. However, the phases of the fundamental tones are kept equal to each other to model one beam. Therefore, the phases of Term 1 and Term 3 are the same as the fundamental tones in the PA outputs. Hence, the inter modulation terms are steered to same direction as the fundamental frequencies as shown in Figure 42. Figure 43 provides simulated results of the combined PA intermodulation patterns and beam with combined PA distortion in-band.

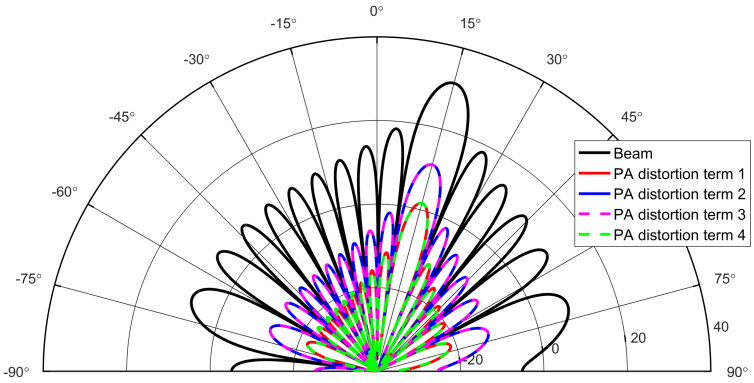

Figure 42. Far-field radiation of the fundamental tones and intermodulation components in array two-tone test.

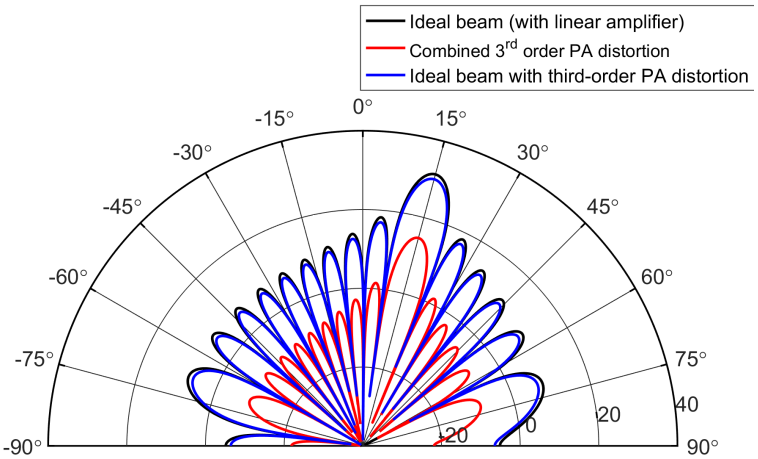

Figure 43. Far-field radiation of the combined third-order distortion and fundamental signal in array two-tone test.

Beamforming coefficients are defined at center frequency. Transmitting any frequency other than center frequency will point in different direction (beam squinting effect). Beam squinting effect increases with steering angle, bandwidth and/or number of elements in uniform linear array (ULA). Intermodulation terms which are away from center frequency will experience more beam squinting effect and will point in different direction than useful beam when useful beam starts steering away from zero angle. Such an effect is illustrated in Figure 44 where the distortion terms steers away from the direction of useful beam because of the beam squinting effect. The effect is very minor because tones are selected near the center frequency and intermodulation are also near the center frequency.

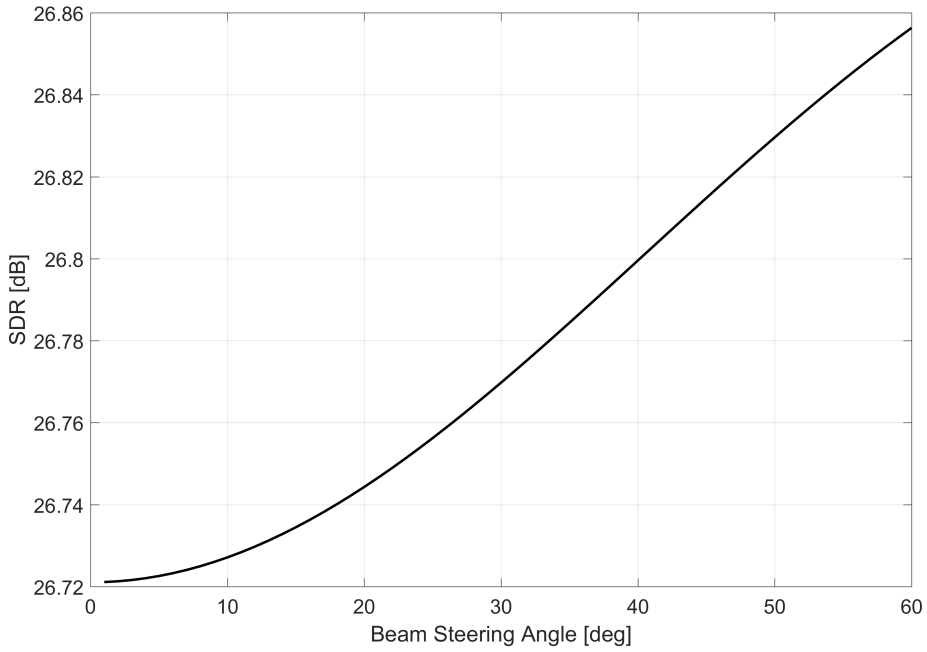

Figure 44. Beam steering angle vs SDR.

5.3. Intermodulation in multibeam transmission

Four-tone signal is used to demonstrate the effects of PA intermodulation in multibeam transmission. In this scenario, two beams are both modelled by two-tone signals which are beamformed to different directions. Hence, there is a four-tone signal in each PA input. PA distortion produces in-band intermodulation terms. Output spectrum of the PA is shown in Figure 45 and the PA generated intermodulation terms are given in Table 4.

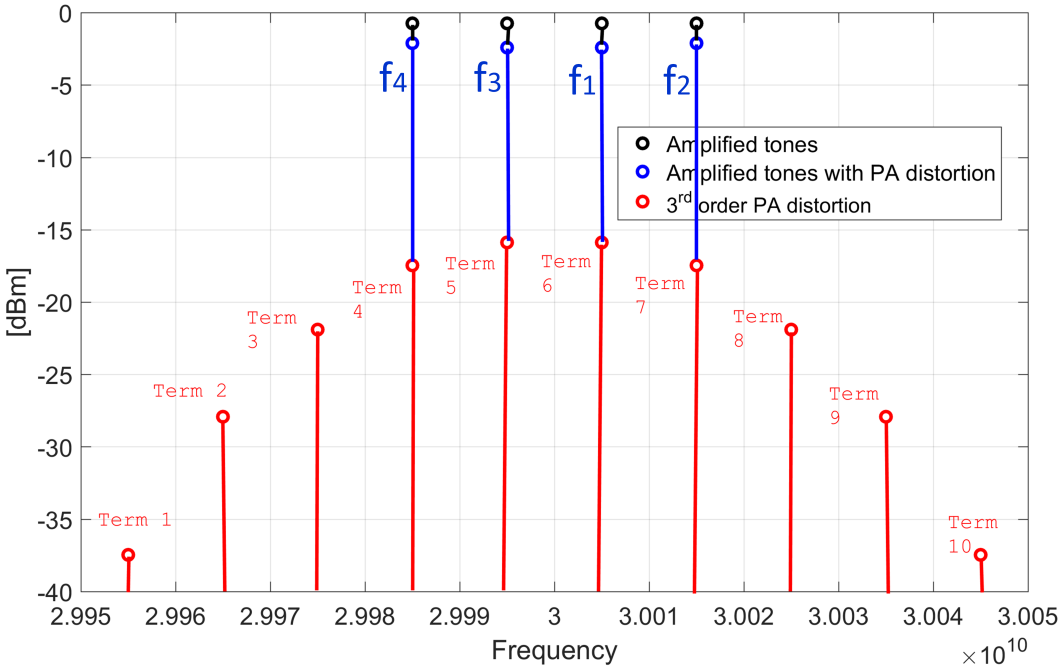

Figure 45. In-band 3^{rd} order nonlinear terms (four tones)

Table 4. In-band 3^{rd} order nonlinear terms (four tones)

Index	**Frequency**	**Phase**
Term 1	$(2f_4 - f_2)$	$(2\theta_4 - \theta_2)$
Term 2	$(2f_4 - f_1)$	$(2\theta_4 - \theta_1)$
Term 3	$(2f_3 - f_2)$, $(2f_4 - f_3)$, $(f_1 - f_2 + f_4)$	$(2\theta_3 - \theta_2)$, $(2\theta_4 - \theta_3)$, $(\theta_1 - \theta_2 + \theta_4)$
Term 4	$(f_1 - f_2 + f_3)$, $(2f_3 - f_1)$	$(\theta_1 - \theta_2 + \theta_3)$, $(2\theta_3 - \theta_1)$
Term 5	$(2f_1 - f_2)$, $(f_1 - f_3 + f_4)$	$(2\theta_1 - \theta_2)$, $(\theta_1 - \theta_3 + \theta_4)$
Term 6	$(2f_3 - f_4)$	$(2\theta_3 - \theta_4)$
Term 7	$(2f_1 - f_3)$, $(f_1 + f_3 - f_4)$	$(2\theta_1 - \theta_3)$, $(\theta_1 + \theta_3 - \theta_4)$
Term 8	$(2f_2 - f_1)$, $(2f_1 - f_4)$, $(f_2 + f_3 - f_4)$, $(f_1 + f_2 - f_3)$	$(2\theta_2 - \theta_1)$, $(2\theta_1 - \theta_4)$, $(\theta_2 + \theta_3 - \theta_4)$, $(\theta_1 + \theta_2 - \theta_3)$
Term 9	$(2f_2 - f_3)$, $(f_1 + f_2 - f_4)$	$(2\theta_2 - \theta_3)$, $(\theta_1 + \theta_2 - \theta_4)$
Term 10	$(2f_2 - f_4)$	$(2\theta_2 - \theta_4)$

When analyzing the four-tone signal, X_{array1} is the two-tone signal defining one beam in one direction and X_{array2} the other two-tone signal defining second beam in different direction. In frequency domain, they can be written as

$$X_{array1} = A_{tones1}[\delta(f_c + \triangle f/2) + \delta(f_c + 3\triangle f/2)],$$
$$X_{array2} = A_{tones2}[\delta(f_c - \triangle f/2) + \delta(f_c - 3\triangle f/2)]\cdot$$

X_{array1} is beamformed by $w_1 n$ in one direction and X_{array2} is beamformed in other direction by $w_2 n$. The beamforming coefficient first and second beam in n:th antenna can be expressed as

$$w_{1n} = g_{1n} e^{j\phi_1 n},$$
$$w_{2n} = g_{2n} e^{j\phi_2 n}.$$

For multibeam scenario, system model in Figure 46 is modelled as fully connected hybrid beamforming architecture. However, the phenomena exist in any architecture where several independent signals are combined before nonlinear PA. In this system, the coefficients for both beams are combined before the PA and fed to all of the antennas. X_n is the input of the nth PA and y_n is the input of nth antenna. For four tones, X_n and y_n are given as

$$X_n = X_{1n} + X_{2n} = w_{1n} X_{array1} + w_{2n} X_{array2},$$

$$\begin{aligned} y_n &= f_{PA_n}(X_n) \\ &= f_{PA_n}(w_{1n} A_{tones1}[\delta(f_c + \triangle f/2) + \delta(f_c + \triangle 3f/2)] \\ &+ w_{2n} A_{tones2}[\delta(f_c - \triangle f/2) + \delta(f_c - \triangle 3f/2)], \end{aligned} \tag{17}$$

where f_{PA_n} is n^{th} power amplifier defined in equation (14). AF in equation (16) is used to demonstrate the effects of PA nonlinearity in beamforming system. Fundamental tones are beamformed and transmitted over-the-air. Figure 47 shows the multibeam pattern along with distortion patterns. Array factor is modelled in Matlab to demonstrate the multibeam patterns and nonlinearity effects on beam pattern.

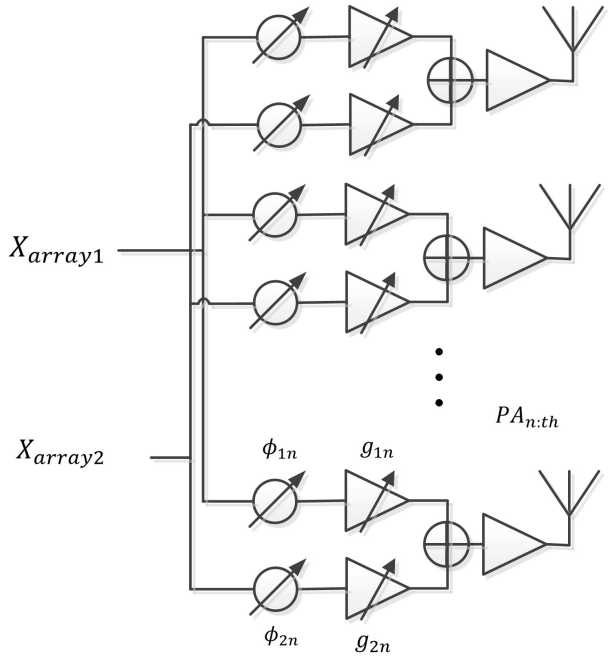

Figure 46. System model for multi-tone multibeam test.

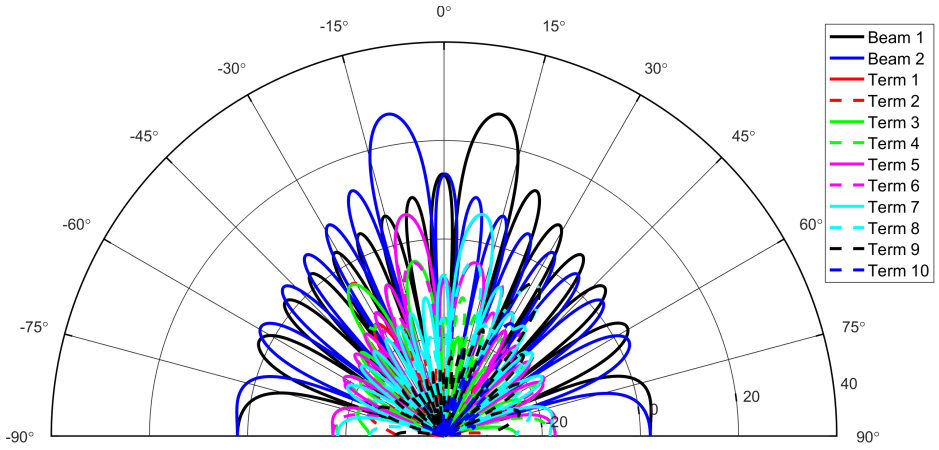

Figure 47. Multiple beams and in-band PA distortion terms.

Intermodulation terms 4, 5, 6 and 7 fall in the same direction as useful beam and cause gain compression for useful beam shown in Figure 48. The nonlinear terms (Term 1,2,3,8,9,10) make similar pattern as fundamental tones because beamforming coefficients are same for fundamental tones and distortion terms. These distortion patterns fall into the direction of sidelobe of useful beam and change the sidelobe levels of the main beam. Higher sidelobes of one beam interfere with other beam and cause inter-beam-interference (IBI) shown in Figure 49. Terms 3 and 9 are composed from several components as shown in the table 4. This is why therm 3 seems to have two beams inside.

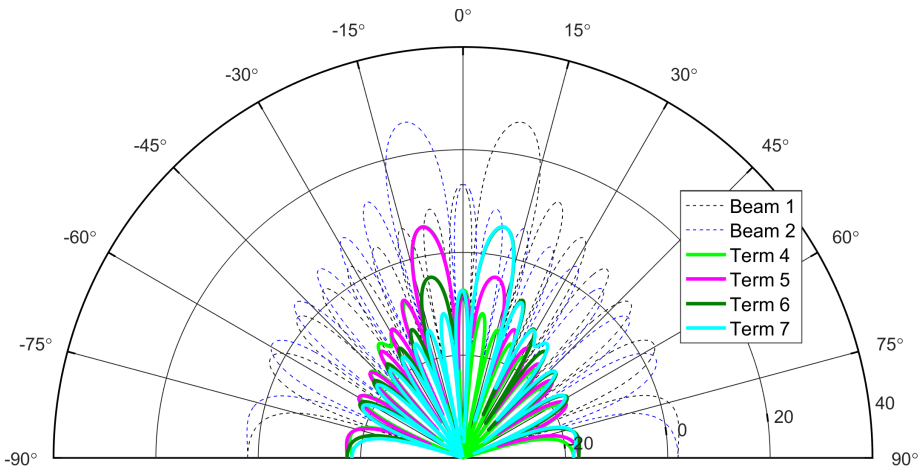

Figure 48. Multiple beams and PA distortion with same frequency.

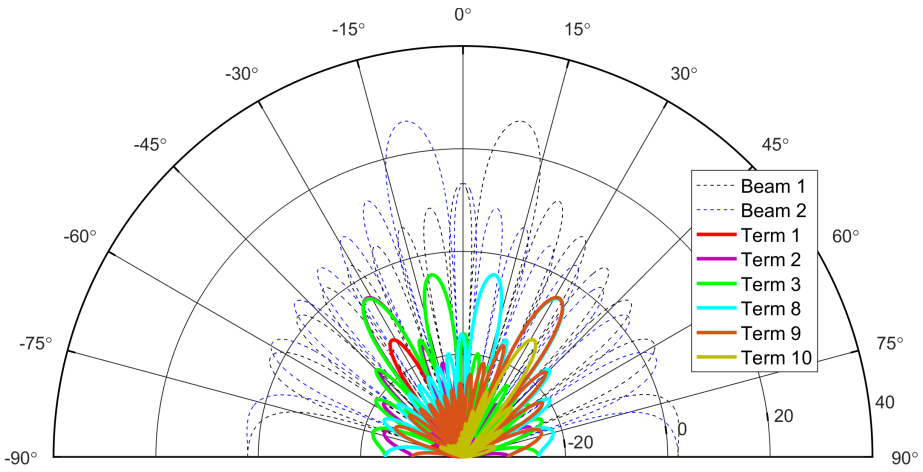

Figure 49. Multiple beams and PA distortion with different frequency.

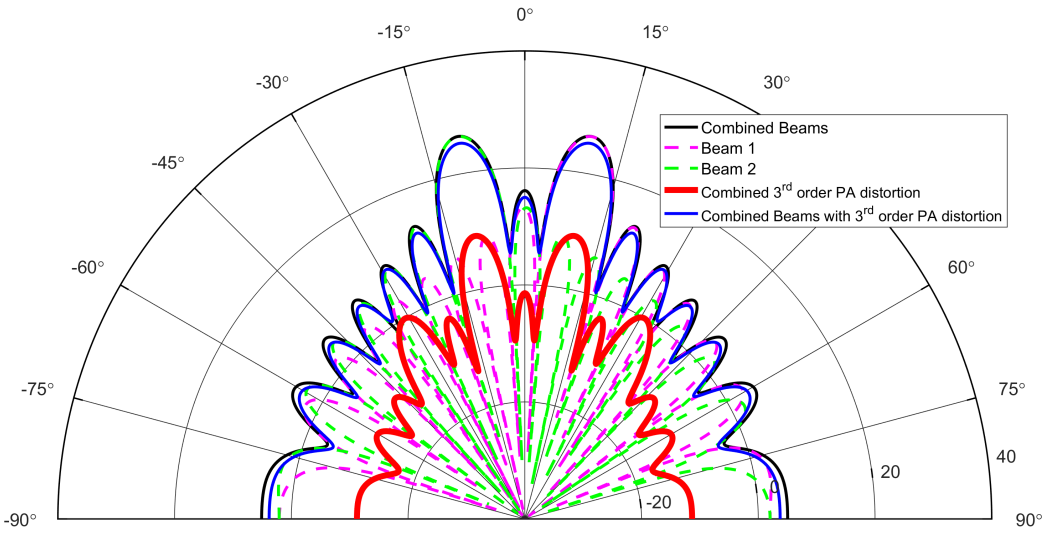

Figure 50. Multiple beams and combined PA distortion.

Array patterns of separate and combined beams with PA distortion are presented in Figure 50. PA nonlinearity degrades the performance in multibeam transmission by reducing the gain of useful beams and changing the sidelobe levels, which in turn increase the inter-beam-interference (IBI). Figure 51 shows the distortion behavior when useful signal beams change their directions, intermodulation patterns also change their directions because phase of intermodulation terms depend on the phase of fundamental frequencies. Distortion patterns are steered to unharmful direction when beams starts steering away from each other. Intermodulation patterns have also nulls and sidelobes like useful beams, which moves away from useful signal direction one after the other. SDR decreases when distortion patterns have their main lobe or sidelobes in the direction of useful beam. SDR increases when nulls of distortion patterns fall in the direction of useful beam. For different separation of beam, SDR changes according to the position of distortion patterns and such analysis is shown in Figure 51.

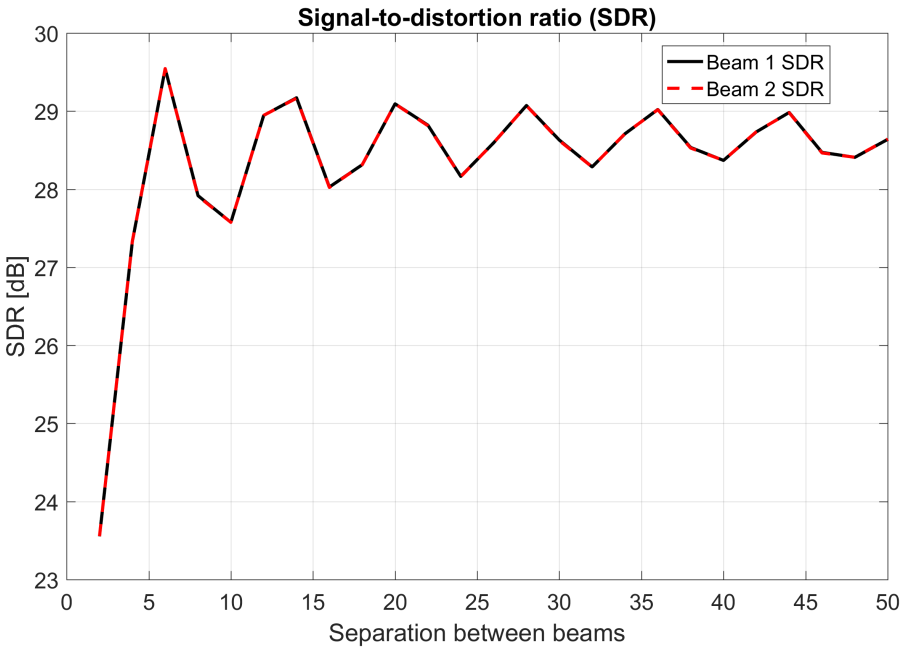

Figure 51. Multiple beams and combined PA distortion.

6. CONCLUSION AND DISCUSSION

In this thesis, phase dependency of IMD on fundamental signals and the behavior of IMD in beamforming system are studied with array two-tone and multi-tone tests. The phase progression of the IMD over the antenna elements is considered to be important in beamforming systems as it eventually makes the beam pattern for the distortion. Based on the polynomial relation of the phase of the IMD with respect to input tone phases, it is expected that the phase progression of distortion depends on the phase of the input tones. This phase dependency of IMD terms with fundamental signal is validated by measurements.

The far-field radiation of the distortion terms are illustrated in both multibeam and single-beam scenarios by utilizing polynomial PA model and array factor. In single-beam case, both input tones has the same phase progression over the antenna elements. Hence, the IMD falls into the same direction as the fundamental tones. However, because of the frequency dependent array behavior, steering angle of IMDs and fundamental tones can vary from the steering angle defined at the center frequency. This effect is called beam squinting and it is concluded to have relatively small impact, if the relative bandwidth of the signal is chosen to be small. However, the effect increases as we increase the tone spacing.

In multi-beam scenario, each beam is modelled by two-tone signal. The phases of the tones are changed for each antenna branch based on the desired steering angle of each beam. The signal seen in each PA input is a multi-tone signal composed on pairs of two tones and each two-tone signal has different phase progression over the antenna elements. Similar frequency-dependent beam squinting effect of IMD terms is seen as it was in single-beam scenario and again the effect is considered to be relatively small with the simulation parameters chosen. In four-tone test, the output will have IMD terms which depends on both of the beams. Hence, the phase progression of these cross-terms depends both of the input beams. Moreover, by simulations it is shown that these terms can potentially fall to other directions than the fundamental signals. The cross terms starts moving away from the useful beam as the separation between beams increases. Therefore, in some cases, the cross terms do not degrade much of the signal-to-distortion ratios of the beams.

In power amplifiers, there is clearly trade-off between linearity and power. Higher linearity can be achieved with fixed power or higher power with fixed linearity. In multi-beams systems, one could drive the PAs potentially harder with multiple beams and still achieve decent signal-to-distortion ratio, as part of the IMD terms are be steered to unharmful directions.

Based on the theory, the spreading of the IMDs terms was expected to be stronger. With some other simulation parameters or higher number of beams we could have shown better results. For multibeam modelling, symmetric frequencies are chosen around the centre frequency, which produces the multiple IMD terms with same frequencies. This makes the distortion analysis challenging as there are several IMD terms in same frequencies, which can potentially affect to each other. In order to understand better the behavior of phase of IMD terms in beamforming system, non-symmetric frequencies are recommended. To have even more reliable demonstration on the array IMD effects for the signal quality, we could have used modulated signals and measure EVM instead of IMD levels. This kind of analysis is shown for example in [29], which demonstrates

the steering the of distortion components to unharmful directions by simulating EVM of the individual streams. In future work, more extensive analysis might be conducted based on the lessons learned in this thesis.

7. REFERENCES

[1] Marchetti N. (2017) Towards the 5th generation of wireless communication systems. arXiv preprint arXiv:1702.00370 .

[2] Osseiran A., Braun V., Hidekazu T., Marsch P., Schotten H., Tullberg H., Uusitalo M.A. & Schellman M. (2013) The foundation of the mobile and wireless communications system for 2020 and beyond: Challenges, enablers and technology solutions. In: Vehicular Technology Conference (VTC Spring), 2013 IEEE 77th, IEEE, pp. 1–5.

[3] Weiler R.J., Keusgen W., Nguyen H.A. & Peter M. (2014) On the choice of carrier frequency and bandwidth for 5g small cell deployments. In: Personal, Indoor, and Mobile Radio Communication (PIMRC), 2014 IEEE 25th Annual International Symposium on, IEEE, pp. 867–871.

[4] Rappaport T.S., Sun S., Mayzus R., Zhao H., Azar Y., Wang K., Wong G.N., Schulz J.K., Samimi M. & Gutierrez F. (2013) Millimeter wave mobile communications for 5g cellular: It will work! IEEE access 1, pp. 335–349.

[5] Pi Z. & Khan F. (2011) An introduction to millimeter-wave mobile broadband systems. IEEE communications magazine 49.

[6] Huang K.C. & Wang Z. (2011) Millimeter wave communication systems, vol. 29. John Wiley & Sons.

[7] Commission F.C. et al. (1997) Millimeter wave propagation: spectrum management implications. Bulletin 70, pp. 1–24.

[8] Rusek F., Persson D., Lau B.K., Larsson E.G., Marzetta T.L., Edfors O. & Tufvesson F. (2013) Scaling up mimo: Opportunities and challenges with very large arrays. IEEE Signal Processing Magazine 30, pp. 40–60.

[9] Rowell C. & Han S. (2015) Practical large scale antenna systems for 5g cellular networks. In: Wireless Symposium (IWS), 2015 IEEE International, IEEE, pp. 1–4.

[10] Vook F.W., Ghosh A. & Thomas T.A. (2014) Mimo and beamforming solutions for 5g technology. In: Microwave Symposium (IMS), 2014 IEEE MTT-S International, IEEE, pp. 1–4.

[11] Samoska L.A. (2011) An overview of solid-state integrated circuit amplifiers in the submillimeter-wave and thz regime. IEEE Transactions on Terahertz Science and Technology 1, pp. 9–24.

[12] Russell K.J. (1979) Microwave power combining techniques. IEEE Transactions on Microwave Theory and Techniques 27, pp. 472–478.

[13] Islam M.S., Jessy T., Hassan M.S., Mondal K. & Rahman T. (2016) Suitable beamforming technique for 5g wireless communications. In: Computing, Communication and Automation (ICCCA), 2016 International Conference on, IEEE, pp. 1554–1559.

[14] Han S., Chih-Lin I., Xu Z. & Rowell C. (2015) Large-scale antenna systems with hybrid analog and digital beamforming for millimeter wave 5g. IEEE Communications Magazine 53, pp. 186–194.

[15] Bogale T.E. & Le L.B. (2015) Massive mimo and millimeter wave for 5g wireless hetnet: Potentials and challenges. arXiv preprint arXiv:1510.06359 .

[16] Iofedov I. & Wulich D. (2015) Mimo–ofdm with nonlinear power amplifiers. IEEE Transactions on Communications 63, pp. 4894–4904.

[17] Ippolito Jr L.J. (1986) Attenuation by atmospheric gases. In: Radiowave Propagation in Satellite Communications, Springer, pp. 25–37.

[18] Mailloux R.J. (2005) Phased array antenna handbook, vol. 2. Artech House Boston.

[19] Understanding 5g beamforming system architecture (accessed 10.02.2017). URL:http://esldesignnotebook.blogs.keysight.com/understanding-5g-beamforming-system-architecture/.

[20] Wu S. Reconfigurable Hybrid Beamforming Architecture for Millimeter Wave Radio: A Tradeoff between MIMO Diversity and Beamforming Directivity. MeidaTek-NTU Research Center .

[21] Jantunen P., Modelling of nonlinear power amplifier for wireless communications (accessed 10.08.2017) (2004).

[22] Amplifier classes and the classification of amplifiers (accessed 1.02.2017). Http://www.electronics-tutorials.ws/amplifier/amplifier-classes.html.

[23] Vuolevi J. & Rahkonen T. (2003) Distortion in RF power amplifiers. Artech house.

[24] Pedro J.C. & Carvalho N.B. (2002) Intermodulation distortion in microwave and wireless circuits. Artech House.

[25] Power amplifier and front end module requirements for ieee 802.11n applications (accessed 12.03.2017). URL: http://highfreqelec.summittechmedia.com/Sep11/HFE0911_Guo.pdf/.

[26] Gharaibeh K.M., Gard K.G. & Steer M.B. (2004) Accurate estimation of digital communication system metrics-snr, evm and/spl rho/in a nonlinear amplifier environment. In: Microwave Measurements Conference, Fall 2004. 64th ARFTG, IEEE, pp. 41–44.

[27] (2013) Rohdeschwarz, lte system specifications and their impact on rf base band circuits (accessed 15.06.2017) URL: https://cdn.rohde-schwarz.com/pws/dl_downloads/dl_application/application_notes/1ma221/1MA221_1e_LTE_system_specifications.pdf.

[28] Cripps S.C. (1999) RF power amplifiers for wireless communications. Artech House.

[29] Tervo N., Aikio J., Tuovinen T., Rahkonen T. & Paerssinen A. (2016) Effects of pa nonlinearity and dynamic range in spatially multiplexed precoded mimo systems. In: 22th European Wireless Conference, pp. 1–6.

[30] Low noise amplifier zfl-500ln (accessed 22.09.2017). URL:https://ww2.minicircuits.com/pdfs/ZFL-500LN.pdf.

8. APPENDICES

8.1. Matlab Script for the measurements.

```
%% parameters for Signal Generator 1
address_sg1 = 1;
sg1 = instrfind('Type','gpib', 'BoardIndex',0,...
    'PrimaryAddress',address_sg1,'Tag','');
power_sg1 = -25;    % Signal Generator 1 power in dBm
frequency_sg1 = 200;% Signal Generator 1 Frequency in MHz
phase_sg1=0;        % Signal Generator 1 phase in degrees
% Signal Generator 1
if isempty(sg1)
    sg1 = gpib('NI', 0, address_sg1);
else
    fclose(sg1);
    sg1 = sg1(1);
end
% Connect to instrument object, sg1.
fopen(sg1);
% Communicating with instrument object, sg1.
% Carrie Frequency
fprintf(sg1,sprintf('CFRQ:VALUE %dMHZ\n',frequency_sg1));
% Power units
fprintf(sg1, 'RFLV:UNITS DBM');
% Power Level
fprintf(sg1, sprintf('RFLV:VALUE %d \n', power_sg1));
% Phase
fprintf(sg1, sprintf('CFRQ:PHASE %d \n', phase_sg1));
%% parameters for Signal Generator address 2
address_sg2 = 2;
sg2 = instrfind('Type', 'gpib', 'BoardIndex', 0,...
    'PrimaryAddress', address_sg2, 'Tag', '');
power_sg2 = -25;      % Signal Generator 2 power in dBm
frequency_sg2 = 210; %  Frequency in MHz
% Signal Generator 2
if isempty(sg2)
    sg2 = gpib('NI', 0, address_sg2);
else
    fclose(sg2);
    sg2 = sg2(1);
end
% Connect to instrument object, sg2.
fopen(sg2);
% Communicating with instrument object, sg4.
% Carrie Frequency
fprintf(sg2,sprintf('CFRQ:VALUE %dMHZ\n',frequency_sg2));
```

```
% Power Level
fprintf(sg2, 'RFLV:UNITS DBM');
% Power Level
fprintf(sg2, sprintf('RFLV:VALUE %d \n', power_sg2));
%% Parameters for Signal Analyzer 3
address_sg3 = 3;
sg3 = instrfind('Type', 'gpib', 'BoardIndex', 0,...
    'PrimaryAddress', address_sg3, 'Tag', '');
% Signal Generator 3
if isempty(sg3)
    sg3 = gpib('NI', 0, address_sg3);
else
    fclose(sg3);
    sg3 = sg3(1);
end
% Connect to instrument object, sg3.
fopen(sg3);
idx= [];
r=1;
for tone = 1:4
    obj1 = instrfind('Type', 'gpib', 'BoardIndex', 0,...
        'PrimaryAddress', 28, 'Tag', '');
    if isempty(obj1)
        obj1 = gpib('NI', 0, 28);
    else
        fclose(obj1);
        obj1 = obj1(1);
    end
    % Input Buffer Size
    set(obj1,'InputBufferSize',3000000);
    % Setting Timeout for function
    set(obj1,'Timeout',1);
    fopen(obj1);
    % Center Frequency
    fprintf(obj1, 'SENSe:FREQuency:CENTer 205MHz');
    % RF Input Attenuation
    fprintf(obj1, 'INPut:ATTenuation 10');
    % Frequency Offset
    fprintf(obj1, 'SENSe:FREQuency:SPAN 50MHz');
    % Ref Level
    fprintf(obj1, 'DISPLAY:TRACE:Y:RLEVEL 0dBm');
    % Set the data trace format to REAL, 32 bits
    fprintf(obj1,':FORM:BORD NORMAL');
    fprintf(obj1,':FORM:DATA REAL,32');
    fprintf(obj1,':INIT:CONT OFF');
    fprintf(obj1,':INIT:IMM; *WAI');
    pause(2);
```

```
fprintf(obj1, 'TRAC? TRACE1');
data = binblockread(obj1, 'float32');
[pk, lc1] = findpeaks(data,...
'MinPeakHeight',-65,'MinPeakWidth',10);
lc=[2*frequency_sg1-frequency_sg2;...
frequency_sg1;frequency_sg2;...
2*frequency_sg2-frequency_sg1];
f_sg30 = lc(tone);
pause(2)
p1_sg30 = pk(tone);
pause(2)
phase_sg30=0;
% Communicating with instrument object, sg3.
% Carrie Frequency
fprintf(sg3, sprintf('CFRQ:VALUE %dMHZ\n', f_sg30));
% Power units
fprintf(sg3, 'RFLV:UNITS DBM');
% Power Level
fprintf(sg3, sprintf('RFLV:VALUE %d \n', p1_sg30));
%% turning off the Sg1 and Sg2 to get peak of Sg3
fprintf(sg1, sprintf('RFLV:OFF'));
fprintf(sg2, sprintf('RFLV:OFF'));
pause(2)
%% Signal Analyzer (Find the peak of Signal Generator 3)
fprintf(obj1,':INIT:IMM; *WAI');
pause(1);
fprintf(obj1, 'TRAC? TRACE1');
data_sg3 = binblockread(obj1, 'float32');
[pk_sg3, lc1_sg3]=...
findpeaks(data_sg3,...
'MinPeakHeight',-65,'MinPeakWidth',10);
%% Update the Signal Generator 30
dif=max(pk_sg3)- pk(tone);
p1_sg30=p1_sg30 - dif;
% Power Level
fprintf(sg3, sprintf('RFLV:VALUE %d \n', p1_sg30));
%% Turning On the Signal Generator 1 and 2
fprintf(sg1, sprintf('RFLV:ON'));
fprintf(sg2, sprintf('RFLV:ON'));
pause(2)
%%  Sweeping inter-tone phase difference
col=1;
sp_start = 0;       % initial phase
sp_step = 10;       % phase step
sp_end = 90;        % end phase

for k = sp_start:sp_step:sp_end
```

```
        fprintf(sg2, sprintf('CFRQ:PHASE %d \n', k)); % Phase
        %% Sweeping the Phase of Signal Generator 3
        reso = 1;
        c=1;
        for ind_p30 = 1:reso:360
            fprintf(sg3, sprintf('CFRQ:PHASE %d \n', reso));
            fprintf(obj1,':INIT:IMM; *WAI');
            fprintf(obj1, 'TRAC? TRACE1');
            data = binblockread(obj1, 'float32');
            p1(r,c)= data(lc1(tone))
            c=c+1;
        end
        [mi mv]           =       min(p1(r,:));
        idx(tone,col)=mv
        min_peak(tone,col)= phase_sg30+mv
        r=r+1; col=col+1;
        % Phase resetting
        fprintf(sg2, sprintf('CFRQ:PHASE %d \n', -k));
        pause(2);
    end
    fclose(obj1);
    clear obj1;
    pause(1)
end
%% Plotting
hold on
plot(sp_start:sp_step:sp_end, idx(1,:));
plot(sp_start:sp_step:sp_end, idx(2,:));
plot(sp_start:sp_step:sp_end, idx(3,:));
plot(sp_start:sp_step:sp_end, idx(4,:));
title('index plot');
%% Closing and Clearing the Objects
% closing signal generator 1 object
fclose(sg1);
% clearing signal generator 1 object
clear sg2;
% closing signal generator 2 object
fclose(sg2);
% clearing signal generator 2 object
clear sg4;
% closing signal generator 3 object
fclose(sg3);
% clearing signal generator 3 object
clear sg30;
```